The Characterisation of Deep-Ultraviolet Ultrafast Pulses by Active Synchronisation via Balanced Cross-Correlation

By

Adam Oliver Sharp

A thesis submitted to Macquarie University

for the degree of Master of Research

Department of Physics and Astronomy

December 2015

MACQUARIE
University
SYDNEY·AUSTRALIA

Examiner's Copy

Typeset in LaTeX 2_ε.

Except where acknowledged in the customary manner, the material presented in this thesis is, to the best of my knowledge, original and has not been submitted in whole or part for a degree in any university.

Adam Oliver Sharp

Acknowledgements

I thank my supervisors and mentors David Coutts, David Spence, and Ondrej Kitzler for their patience, teaching, and optical wizardry that has continued to impress and inspire me during this challenging thesis. I would also like to acknowledge Chris Artlett, who provided some of his PMT equipment which was invaluable for the progression of this research.

Abstract

This thesis details techniques necessary for the characterisation of the deep UV output from mode-locked cerium lasers. Previously 6 ps pulses have been obtained from an 80 MHz Ce:LiCAF laser, but these pulses are likely to have been chirped given there was no intracavity dispersion control. Full characterisation, using techniques such as frequency resolved optical gating (FROG), is needed to further develop these novel solid-state ultraviolet laser systems to their full potential as femtosecond or even attosecond lasers.

The most appropriate technique for characterisation of deep UV ultrafast pulses is to perform synchronous cross correlation FROG (X-FROG) measurements using an auxilliary femtosecond Ti:sapphire laser as a reference. The first steps to achieving this are to synchronise two independent ultrafast lasers: the Ce:LiCAF laser under test with a femtosecond Ti:sapphire laser. Given that the Ce:LiCAF laser is itself synchronously pumped by the 266 nm fourth harmonic from a mode-locked Nd:YVO_4 laser, initial synchronisation of the Ti:sapphire laser to the Nd:YVO_4 laser is suitable for evaluating synchronisation and UV X-FROG techniques.

A femtosecond Ti:sapphire laser was synchronised to an independently running mode-locked Nd:YVO_4 laser using balanced synchronisation techniques, and the timing uncertainties of the synchronisation were evaluated. Synchronous and asynchronous cross-correlation and FROG techniques were employed to evaluate the 266 nm pump laser and Ti:sapphire reference laser ultrafast pulses. This is the key first step to performing such measurements on the output of a cerium laser to allow further optimisation and external pulse compression of this system.

Contents

List of Figures

List of Tables

1

Introduction

Ultrafast lasers have advanced significantly since the first demonstration of a Q-switched mode-locked laser in 1966 using a dye saturable absorber, this laser was capable of pico-second pulses. Today's ultrafast lasers have pulse durations down into the attosecond domain, peak powers up to the PW level, and broad-bandwidths that cover the visible spectrum and beyond. Since the 1960s, a variety of optical designs and gain materials have matured into various continuous-wave and pulsed lasers that are immensely useful and reliable. This has opened up the spectrum for generating previously untapped wavelengths of light, from x-ray to infra-red. Today, the optical properties of lasers are highly tailored to applications that also have practical requirements that include being compact, robust, and simple to use. The desire to improve applications drives the need for easy and versatile methods of generating light, and new sources have opened up new applications. There is the constant need for development and refinement of laser sources and generation techniques to provide a diverse range of technologies that can be combined and fitted to many scientific and industrial applications.

The deep-ultraviolet spectral region covers a wide range of probing applications such

as the manipulation of quantum mechanical systems, and time-resolved transient absorption spectroscopy [4, 5]. Remote detection of chemical and biological agents provides valuable information into photochemical dynamics [4]. This includes the observation of vibrational modes, in ground and excited states, of substances such as thymine. Additionally, resonance spectra of chemical mixtures such as acetylene and nitric oxide have been accessible via tunable pulses. Sub-10 fs pulse durations from deep-ultraviolet (DUV) to near infrared (NIR) [6–8] at pulse repetition frequencies (PRFs) on the order of 100 GHz have provided enormous bandwidth and tunability in these spectral regions to the advantage of spectroscopy and probing of ultrafast processes [9].

Lasers are also increasingly utilised in the field nanobiophotonics for a variety of detection applications including imaging-based techniques relying on light-matter interactions and photoluminescence [10, 11]. Flow cytometry is one such application, which is used to distinguish between and separate biomatter in a flowing capillary via laser light excitation and detection. This technique is used as a marker for sorting and counting of cells and proteins in fluidic channels, that can be manufactured on a microchip scale. Protein inactivation is a similar technique reliant on short laser pulses. Fluorescent materials can have multiple different excitation and emission wavelength combinations which allow for individual or selective activation/excitation of single materials. Again, for this task, tunable lasers with broad gain bandwidths, particularly for the UV-vis-IR region in which many of these biomaterials interact offer, are of significant interest.

In addition to these scientific applications, industrial fabrication processes utilising pulsed lasers include lithography, cold ablation machining, and direct-write waveguides [12, 13]. These are different processes but generally rely on high peak powers for ablation or dielectric modification. That is, the removal of matter or refractive index modification of glass, via ultra-short laser pulses. Ablation involves the ejection of material by incident light pulses, and thus it is desirable to maximise peak intensity in the target volume, to ensure the clean removal of ejecta. UV light is usually used for micromachining for this reason; it is absorbed by most materials easily and offers a small enough focal spot size for precision fabrication. Direct-writing of waveguides involves the focusing of infra-red Ti:Sapphire radiation, into bulk glass or silica for the construction of waveguides, optical switches and couplers, or more complicated photonic structures like photonic lanterns. This utilises a the strong electric field in the focal region for localised refractive index modification. More recently, the fabrication

of micro-fluidics have progressed and to increasingly attractive means of the aforementioned flow cytometry

The emergence of Ti:Sapphire lasers in the 1990s sparked a renaissance in the generation of ultrafast pulses including new methods of ultrafast generation. Of the variety of optical designs and gain materials that have been discovered and utilised, Ti:sapphire remains an industry standard, offering a robust solid-state solution to ultrafast pulse generation at high peak powers. Its success can be attributed to the naturally broad bandwidth of the gain media, the ease of pulse compression methods in this spectral region, and the implementation of Kerr-lens mode locking (KLM) in producing peak powers higher than ever before. A broad bandwidth is necessary to support the short pulse durations; with spectral broadening via self-phase modulation (SPM) from KLM and a broad gain bandwidth, Ti:sapphire is capable of sub-5 fs pulses [14].

The development of other mode-locked lasers rapidly increased in the early 1990s due to the introduction of semiconductor saturable absorber mirrors (SESAMs) which offered a reliable, passive solution [15] to mode-locked lasers that do not comprise a Kerr gain media, such as Neodymium based lasers including Nd:YAG at 1064 nm. For media with sufficient gain bandwidth, modelocking is realised in simple and cost-effective systems to produce tens of Watts of average power at MHz repetition frequencies. These lasers also provide a high powered ultrafast source at frequency multiples 532, 355, and 266 nm by non-linear frequency conversion, the 266 nm being of particular relevance to this thesis. Despite the technical challenges of achieving high average powers in the deep UV by the fourth harmonic generation from Nd lasers, average powers of over 20 W have been achieved. For example, Edgewave recently released a new product that produces 20 W of average power at a PRF of 20 MHz with 10 ps 266 nm pulses for industrial machining applications.

Harmonic generation encapsulates the widely used non-linear generation of optical harmonics from incident light, second harmonic generation (SHG) which can be performed by focusing a single source into a suitable non-linear crystal such as BBO. This birefringent material is implemented for phase-matching the input and output fields ($n_{\lambda 1} \approx n_{\lambda 2}$) for efficient conversion between harmonics. This would not occur normally due to chromatic dispersion, however the refractive index of birefringent crystals is also polarisation dependent so there is an angle at which both beams may propagate at equal index. Sum-frequency generation (SFG) and difference-difference frequency generation (DFG) are similar processes involving

three wavelengths of light instead of two as in SHG; the generation of harmonics that are equal to the *sum* of, or *difference* between the energy of the two input wavelengths. Additionally, these can be further divided into type-1 and type-2 phasematching where the lower energy wavelengths have the same and opposite polarisation respectively.

The deep-ultraviolet (DUV) spectral region is one with many applications, yet has few means of practical generation. Many of the current methods of generating ultra-short pulses in this region rely on non-linear harmonic generation of a Titanium:sapphire with itself or another laser. The Ti:sapphire gain material has a broad gain bandwidth (650 - 1100 nm), which makes it highly suited to ultra-fast applications. For example, third harmonic conversion from 780 nm to 260 nm is readily obtained from Ti:Sapphire lasers. This converts the IR tunable/pulsed light to the DUV with a tuning range based on the original Ti:Sapphire tuning bandwidth. However, non-linear conversion to the deep UV for ultrafast lasers is problematic in that only a limited spectral bandwidth is usually converted leading to a lengthening of the laser pulse.

A variety of other UV sources have been developed that include dye lasers, excimer lasers, and the aforementioned frequency quadrupled systems [8, 16]. Raman lasers also offer a relatively versatile method for generating light at new wavelengths [17], for example using diamond as a robust gain material with a high damage threshold. Although not all wavelengths of light can be generated via this technique, all that is required is a high power pump source that satisfies the stokes generation. For example, a frequency quadrupled 266 nm source pumping a 276 nm Raman laser [18]. While many of these light sources can generate DUV wavelengths relatively simply, narrow linewidths limit the potential for their deployment in ultrafast applications [19].

Over the last 40 years, cerium has slowly emerged as a highly suitable ultrafast laser material for DUV applications. It has a gain bandwidth of over 30 nm and thus the potential for femtosecond pulses. The most promising of cerium gain media comprise a robust low loss host material doped with (Ce^{3+}) ions. Solid state systems are durable and simple for practical applications, but in the case of cerium, more significant loss mechanisms that would otherwise prevent lasing were necessarily overcome in the past. This includes excited state absorption and colour centre formation, discussed in the next chapter. These processes are relatively minor in Ce:LiCAF, which permits direct lasing of Ce:LiCAF centred at roughly 290 nm with a bandwidth comparable to Ti:Sapphire [1] in the infra-red. Additionally, the

LiCAF host has been developed into KLM ultrafast lasers for the near-IR; Cr:LiCAF. With no dispersion compensation, pulse durations as short as 6 ps have already been reported for a mode-locked Ce:LiCAF laser [3]. However, the bandwidth provided by Ce:LiCAF can support sub-fs pulses. There is therefore the imperative for investigation into dispersion and subsequent pulse compression for the full potential of direct-DUV ultrafast cerium lasers to be realised.

2

Cerium Lasers

2.1 Introduction

Cerium lasers based on the 5d → 4f transition of trivalent lanthanides were first discussed over 40 years ago by Elias et. al [20]. Since this time, the first cerium laser, demonstrated by Dubinskii et al, was followed by a flurry of research into cerium host materials and cavity designs [21]. The majority of the designs comprised of low PRF Q-switched pump sources, which generate high pulse energies and average powers. These were necessary to overcome various loss mechanisms associated with the energy levels of Ce^{3+} doped crystals. With increasing availability of more powerful and compact pump sources for cerium gain media, the realisation of the femtosecond potential of cerium lasers becomes more important. This section describes the previous research necessary for characterisation and development of basic materials, and cavity designs for directly generating pulsed DUV light.

2.2 Previous research in pulsed cerium lasers

There are several viable host materials for the Ce^{3+} ion that have sufficiently low loss with respect to primary loss mechanisms; excited state absorption and colour centre formation [1]. The characterisation of potential host materials revealed that Ce:LiCAF, Ce:LiSAF, and Ce:LLF are the most promising in terms of loss, efficiency, and bandwidth [22–24]. These will be compared briefly, prior to examination of several systems with Ce:LiCAF as the gain medium.

The nature of cerium is described by the energy level diagram of figure 2.1, which includes the the 5d → 4f laser transition. The large bandwidth of this laser transition is due to broadening of the 4f levels. The nature of loss via excited-state absorption is the excitation to an energy level that exceeds these upper laser levels; the conduction band. It is also possible that decay from an excited state forms a colour centre, which itself can act as an absorber for pump or laser photons. Unfortunately, the net loss in many potential cerium hosts is too high for lasing. It is important to reduce the effect of these two mechanisms, with Ce:LiCAF and Ce:LiLuF emerging as the two most efficient cerium laser materials.

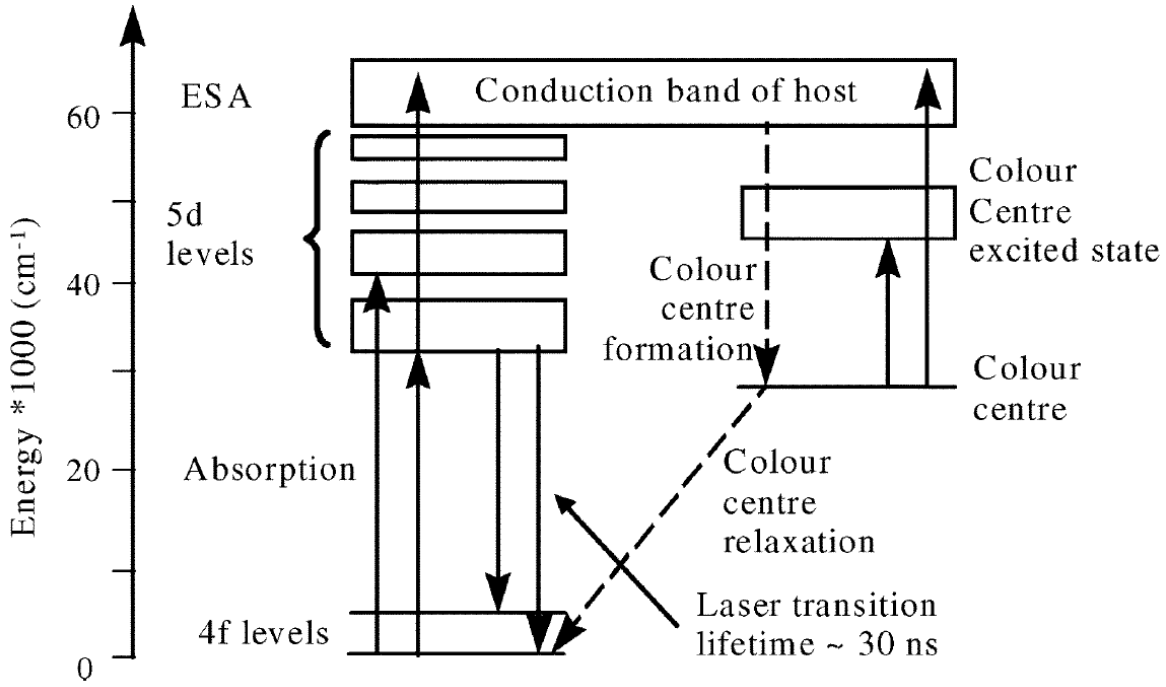

Figure 2.1: Energy level diagram of the 5d to 4f transition for cerium lasing from [1].

Since the discovery of cerium as a suitable dopant in the construction of DUV lasers, pulsed systems ranging from 10 Hz to 1.1 GHz have utilised a variety of cerium laser crystals

[25]. Most cerium media have peak absorption in the region of 250 - 300 nm; Ce:LiCAF and Ce:LiSAF are at approximately 266 nm [1], while Ce:LiLuF's absorption peak is at the 289 nm lasing wavelength of the other two materials.

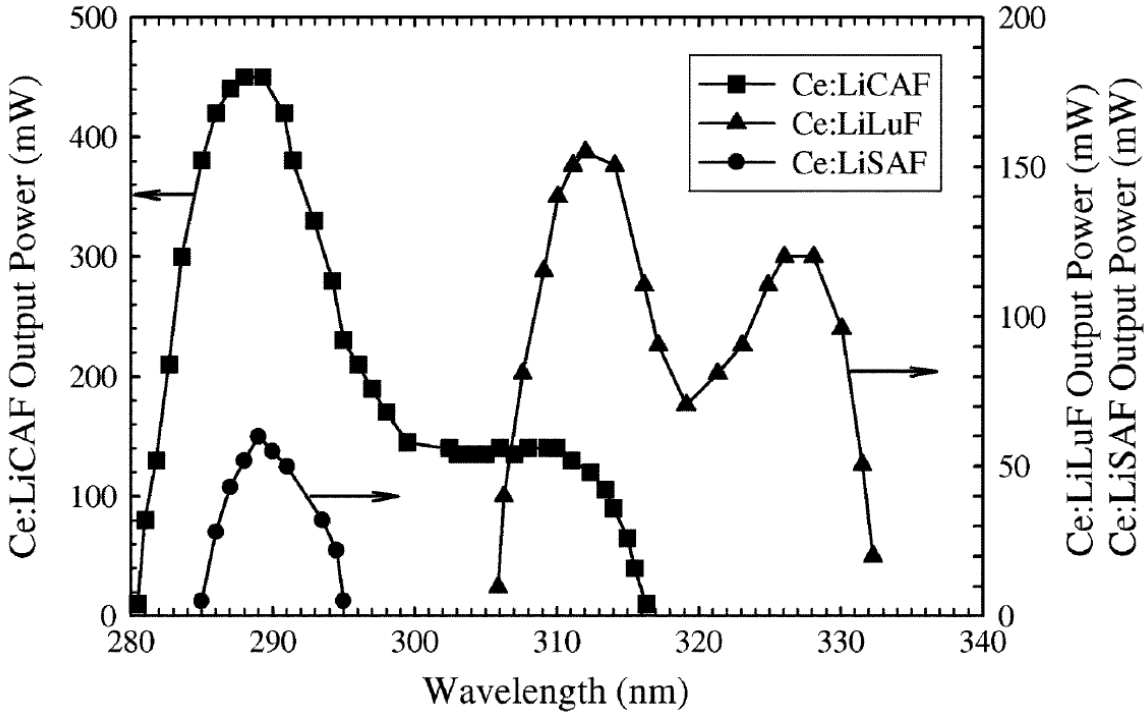

Figure 2.2: Power and spectral output from [1], comparing the overall effectiveness of the most successful cerium media as broad bandwidth DUV sources.

Previously a suitable wavelength for pumping Ce:LiCAF was the 271 nm sum-frequency output from a copper vapour laser operating at 511 nm and 578 nm [26, 27]. This was particularly useful for the characterisation of the various cerium gain media as the CVL provides high average powers at kHz PRFs. The power output of primary cerium media using this pump source is shown in figure 2.2 and distinguishes LiCAF as the most powerful and spectrally broad medium under these conditions. However, the CVL is an immensely cumbersome and expensive solution to pumping Ce:LiCAF which would otherwise be a robust, light weight, and all solid-state laser system.

Cerium materials emit in a broad range from 280 nm to 330 nm and exhibit individual bandwidths of over 30 nm, as well as efficiencies of over 70 %. This includes two of the easily pumped options for the host material of ultrafast cerium lasers; LiCAF and LiSAF, which are centered at approximately 289 nm [1]. This wide bandwidth has the potential to support ultrashort pulse durations of a few femtoseconds. The discovery of new gain media is a very

important aspect of laser development, but highly suitable host materials for cerium have already been developed. It is therefore suitable to optimise cerium lasers based on the best of the established gain media for power, efficiency, spectra, pulse duration, and other aspects necessary for tailoring these systems to a wide range of applications. In achieving these goals, Ce:LiCAF presents the most logical route. It is easily pumped at 266 nm light, has a wider bandwidth than Ce:LiSAF and higher efficiencies, and is a demonstrated KLM host medium with a high damage threshold. The superior performance of Ce:LiCAF positions it as the best candidate to approach the realm of direct fs DUV generation.

Some of the highest average powers of cerium based systems to date have been demonstrated by their use in an amplifier arrangement [2]. Average power outputs at the Watt level have been achievable by pumping of Ce:LiCAF in multi-pass systems that use Q-switched bi-directional pumping schemes. Figure 2.3 shows a particularly elegant method of implementing a Ce:LiCAF crystal as an amplifier seeded by a nanosecond Ce:LiCAF oscillator.

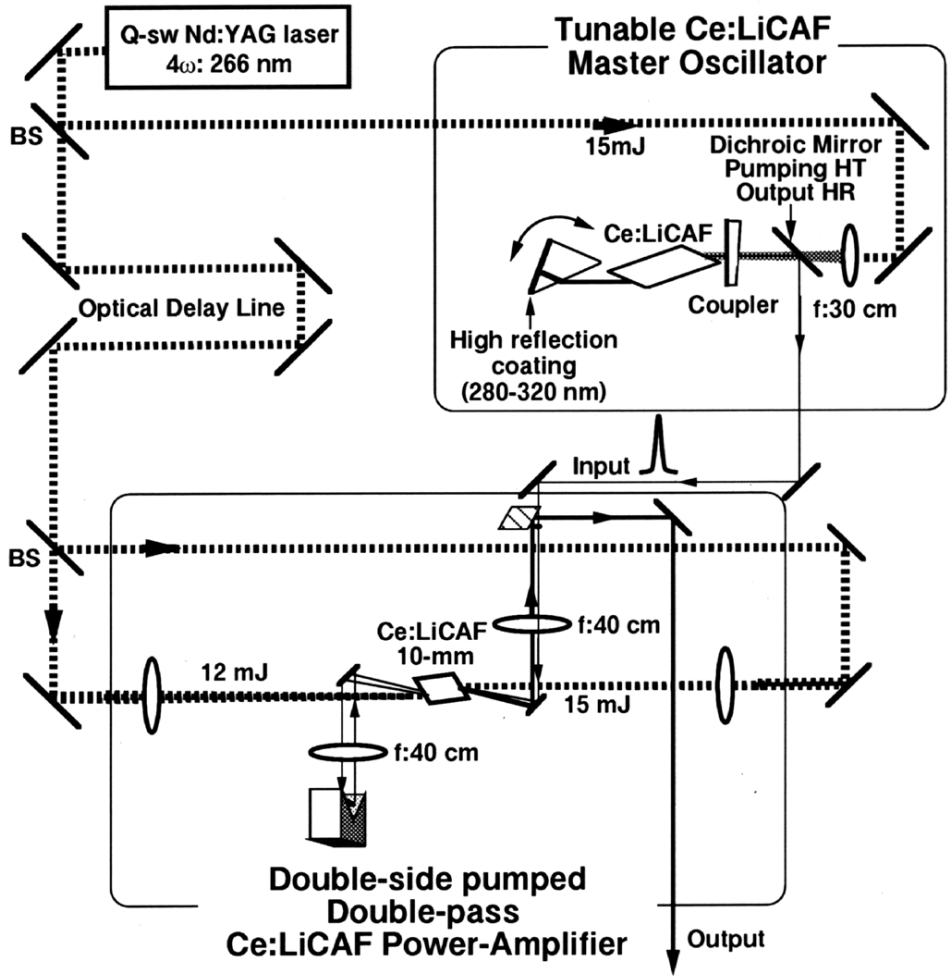

Figure 2.3: A short Q-switched tunable Ce:LiCAF oscillator and amplifier system from [2].

Over the last decade, pulse durations of cerium lasers have entered the picosecond regime by utilising sub-ns microchip pump lasers and very short optical cavities in gain-switched configuration. These systems, while capable of pulses down to several hundred picoseconds, do not have the potential for ultrafast KLM operation. Investment into this area has been motivated by the wide tuning range provided by cerium, and high pulse energies that are generated using this slower technique. The advantage of using Q-switched cavities like these is in compact operation and miniaturisation of pump sources via microchip lasers. However, development into ultrafast oscillators necessitates relatively long cavities with minimal loss, if KLM is to be realised.

2.2.1 Synchronously pumped mode-locked Ce:LiCAF laser

The future of cerium gain media leans on the development of efficient pumping mechanisms for 266 nm light, which is a significant limitation at present due to the low average power capability of most non-linear crystals to generate this fourth-harmonic. The lack of suitable pump lasers is more significant for continuous-wave operation of cerium [28], which is particularly challenging due to its 25 ns upper state lifetime. The most effective means of producing the necessary CW powers lie in cavity enhanced frequency doubling of green lasers. However, higher power CW 266 nm generation is problematic due to thermal effects in the BBO. While thermal effects are also an issue for mode-locked 266 nm laser systems, single-pass frequency conversion of 532 $\rightarrow$ 266 nm light is sufficient for generating the necessary pump powers and is much less sensitive to thermal effects than resonant frequency doubling of a CW green laser.

Developing efficient widely tunable nanosecond cerium laser systems has been the most significant driver for this field, with the potential for high repetition rate (MHz) mode-locked cerium lasers being relatively unexplored. In recent years, the development of Ce:LiCAF saw its first case of mode-locking: a 6 ps pulse duration from a 78 MHz synchronously pumped 3-mirror cavity producing average powers of over 50 mW [3] which have escalated to almost 300 mW as the result of improvements in HR mirrors at these wavelengths [29].

When a mode locked laser is used as a pump source for another laser, there is the option to use synchronous pumping. This is arranged by matching the cavity lengths of the test laser to the pump laser so that the repetition rate is the same for both. This provides time-varying gain to the cavity. As a result, a pulse train builds up quickly, and passively

in self-starting configuration, unlike KLM. Synchronous pumping is somewhat sensitive to cavity length variations, with pulse energy decreasing significantly when moving away from synchronisation. Synchronous pumping does allow for harmonics of the pump laser pulse repetition frequency to be produced. This is detailed in [29] for which a wide range of harmonic PRFs are examined. However, for this work, the 1st harmonic will be sufficient.

2.3 Ultrafast pulse characterisation in the deep ultraviolet

2.3.1 Asynchronous cross-correlation measurement

Many techniques of characterising ultrafast pulses are not applicable in the DUV, and those that may be of use are quite limited. The first reports of synchronous mode-locking a Ce:LiCAF laser include the asynchronous cross-correlation characterisation of pulse durations as low as 6 ps. This was performed using an auxiliary femtosecond mode-locked Ti:sapphire laser with both the Ti:sapphire and Ce:LiCAF lasers operating near 80 MHz and producing a 1-2 kHz beat frequency. This produced a reliable measurement of pulse duration with relative ease. However, asynchronous sampling is a relatively limited method of characterisation whose resolution diminishes for shorter pulse durations as a result of the beat frequency between the two PRFs.

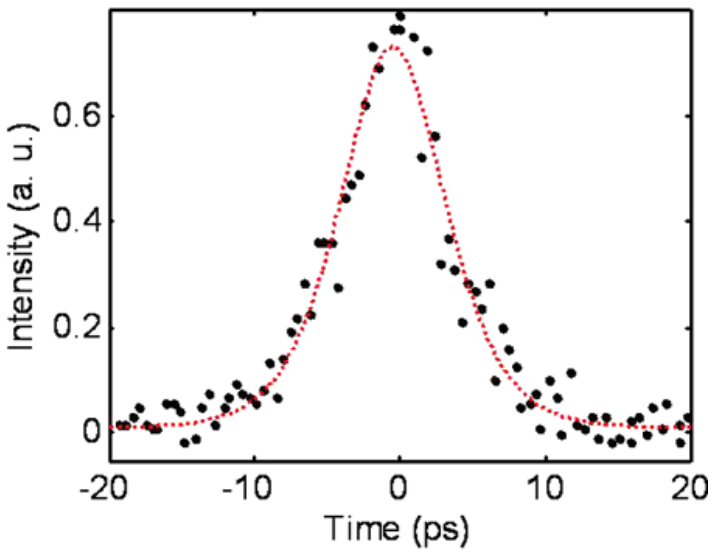

Figure 2.4: Asynchronous cross-correlation of Ce:LiCAF with Ti:sapphire yielding a FWHM of 6 ps from [3].

2.3.2 Spectral characterisation by Frequency Resolved Optical Gating

A laser cavity comprises optical elements that generally exhibit some level of chromatic dispersion. In pulsed systems this can cause temporal broadening of the resonating pulse; increasing the pulse duration. Dispersion causes the spectral components to separate in time in the axis of propagation. The dispersion characteristics of the LiCAF host are in fact several times higher in the ultra-violet than compared with the near-IR region that Cr:LiCAF occupies. Bandwidth measurements of the synchronously pumped Ce:LiCAF laser show that the pulses were not transform limited, and indicate that there is potential for further compression of the 6 ps pulses down into the femtosecond domain.

Dispersion compensation for pulse compression is the next steps in working towards ultrafast direct-DUV pulses. Prism pairs, chirped mirrors, and grating configurations are the primary methods of pulse compression, from which other novel techniques stem [6, 30]. Double prism pairs offer relatively low loss in the DUV and have variable dispersion compensation necessary for the tuning and characterisation [31] of cerium. These are easy to implement external from the cavity and provide a practical basis of second-order dispersion compensation for initial pulse compression experiments. Chirped mirrors provide a convenient solution to intracavity dispersion and aim to induce a strong non-linear Kerr response in the crystal that encourages broadbandwidth ultrashort pulses [32]. Current issues related to chirped mirrors in the DUV are the level of loss associated with them, but over time this is expected to improve. The losses and complexity of diffraction gratings in the DUV make this technique more difficult. Thus, prism pairs offer an ideal starting point. The combination of these techniques is necessary to research and realise the potential of cerium fluoride lasers.

In the process of characterising dispersion in the test cavity, characterisation of the chirped output pulses is sufficient. Frequency resolved optical gating (FROG) provides the spectra and phase information that we seek from this process. It relies on non-linear frequency conversion for time gating, and a variable delay line to scan a probe and test pulse. FROG can be performed using a single laser, with a beam splitter via second harmonic generation (SHG). A delay line temporally scans two pulses through each other and the measurement of this newly generated frequency yields the convolution of the two input pulses. The nature of this technique is dependent on the wavelength of the input source, as a detector at half of this wavelength is needed. In our case, FROG techniques are impractical due to the

transmission bandwidths of most non-linear crystals and the output signal would be in the vacuum ultraviolet which has significant propagation losses. An alternative approach is therefore necessary.

Cross-correlation FROG (XFROG) is a more advanced technique that uses two different input beams and relies on difference or sum frequency generation (DFG/SFG). This technique is advantageous as it can therefore be performed on pulses in the DUV. The ability to measure the spectral content of the pulse requires using active synchronisation of a probe and test pulse. Synchronised characterisation using X-FROG provides a means of integrating for longer periods of time, overcoming the sensitivity limitations of other methods such as asynchronous sampling. Timing error is also lowered as it is a variable of pulse duration, with timing errors generally on the order of 1% of the duration of the longer pulse in the system. Characterisation of DUV relies on DFG to produce a measurable signal, and will rely on synchronisation for X-FROG to function correctly. This is a fantastic tool in the characterisation of DUV [33], if a synchronous probe is available.

2.3.3 Active synchronisation by balanced cross-correlation

Balanced synchronisation is a method of synchronising the repetition rates of two lasers so that their pulse trains overlap in time. The technique requires a two-arm module with some form of wave-mixing in each to produce a cross-correlation signal. In one of the arms, the pulses are delayed relative to one another as shown in figure 2.5.

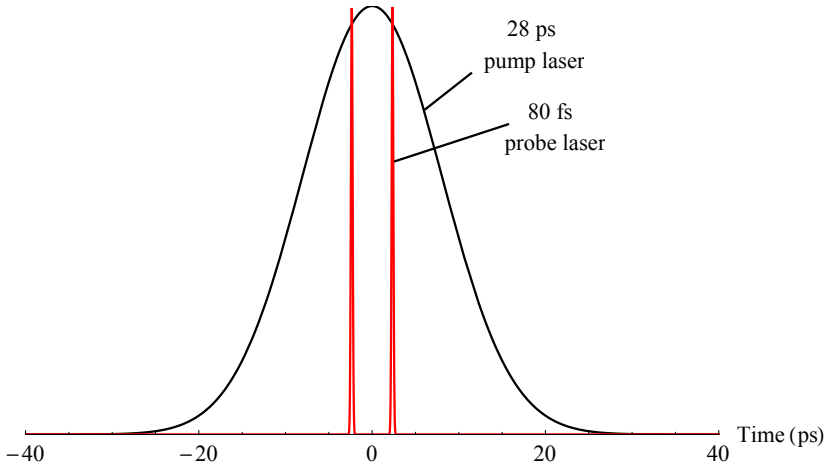

Figure 2.5: Balanced synchronisation using two arms, one with a 5 ps relative delay between the 1064 nm pump and 800 nm probe pulses used in this experiment.

The separate arms generate a signal, typically via SFG or DFG, at a fraction of the maximum that would be generated for perfectly overlapped pulses. The difference between these two signals is then used in a feedback loop that adjusts the cavity length of one of the lasers. The geometry of a Gaussian that describes the carrier of the pulse is therefore utilised as a means of providing a balanced signal in a synchronised feedback loop.

Although they are not the only option, photodiodes (PDs) are commonly used devices for the detection of the balanced signal; they have a fast rise time that improves responsiveness and the material can be selected so that only the balanced signal is within the spectral response range, effectively reducing noise. Fluctuation of the synchronisation system causes an inevitable timing error between pulses, with the error of an effective system able to reach values lower than 1% of the test pulse duration. For example, an RMS of 300 as for a pulse duration of 45 fs was reported in [34], while other results achieve errors as low as 83 as for similar pulses. This technique is therefore highly suited for X-FROG techniques, which demands precise timing of optical pulses, as the timing error is likely to be significantly lesser than the current pulse duration of 6 ps.

3

Synchronous characterisation in the DUV region

3.1 Introduction

In order to characterise the ultrafast output of a mode-locked Ce:LiCAF laser using XFROG it is necessary to synchronise the cerium laser with a mode-locked fs Ti:sapphire laser In this chapter, experimental details of the synchronously pumped mode-locked cerium laser are presented together with experimental details of locking the Nd pump laser to a fs Ti:sapphire laser and the X-FROG measurement technique.

At the start of this project, a Nd:YVO_4 laser and its frequency quadrupling stage to produce 266 nm light was already constructed together with a Ce:LiCAF oscillator. This occupied the full width of an optical table. Figure 3.1 shows the beam path layout that was designed with simultaneous synchronisation and characterisation of the Ce:LiCAF oscillator in mind. For this aim, an ultrafast Ti:sapphire pumped by 532 nm CW radiation was positioned so

that the output beam could be split into: a combining mirror with the Nd:YVO_4 pump for synchronisation via balanced cross-correlation, and insertion into a FROG or X-FROG system for spectral analysis of the Ce:LiCAF oscillator. Also on the table was a nanosecond Ce:LiCAF alignment laser, itself pumped by a frequency quadrupled Nd:YAG microchip laser (Alphalas).

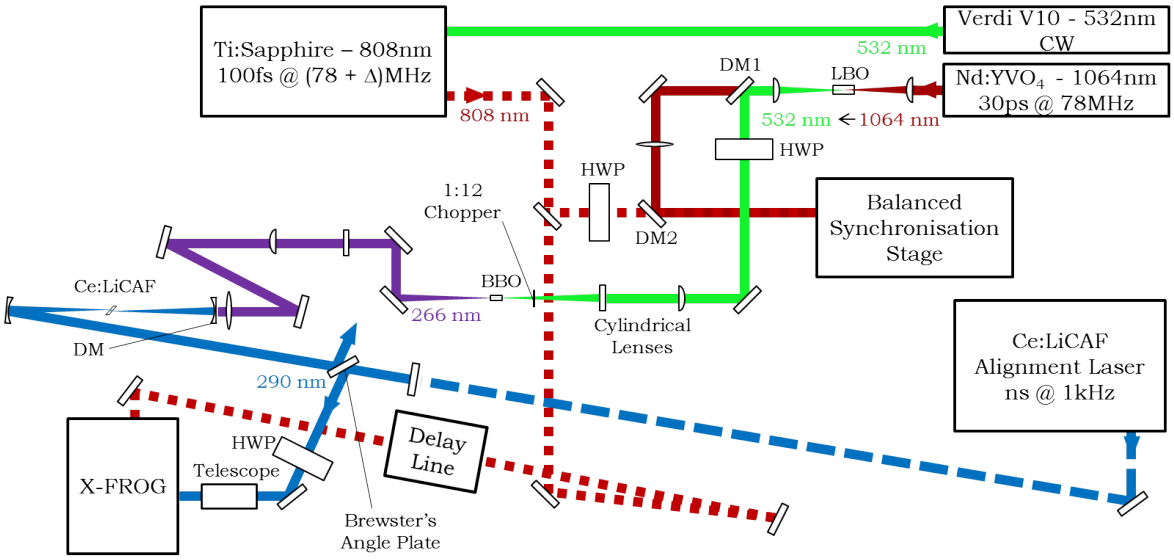

Figure 3.1: The designed optical layout for obtaining X-FROG measurements of the 290 nm Ce:LiCAF test laser using an 808 nm probe Ti:sapphire laser. DM: Dichroic Mirror.

The layout of figure 3.1 was initially intended to provide synchronisation between the 290 nm Ce:LiCAF test laser and 808 nm probe directly as it provides the most accurate synchronisation. The Brewster-plate output coupler in the Ce:LiCAF cavity conventionally offers output in two directions; one for synchronisation and the other for characterisation. However, with a 12:1 duty cycle due to the thermal limitations of the BBO for 266 nm generation, an optical chopper was inserted in the pump laser beam path. However, a chopped signal may place significantly more dependence on a fast locking scheme, and as this had yet to be constructed, an alternative route was devised.

The chopper was moved from its original location, behind the LBO crystal, to immediately in front of the BBO crystal. This removes the chopper envelope for both the waste 1064 nm light and leaked 532 nm light that pass through the first dichroic turning mirror. These are suitable sources for synchronisation as they provide an uninterrupted sum frequency signal. At a later stage, once the chopper is removable, direct synchronisation to the Ce:LiCAF laser may be useful in improving performance, but is not examined in this work.

3.2 Frequency quadrupled Nd:YVO_4 pump laser

The SESAM mode-locked Nd:YVO_4 laser in the right of figure 3.1 achieved maximum average powers of 26 W at 1064 nm with a pulse duration of 28 ps and a PRF of roughly 78.6 MHz. This pump source was focused into a 35 mm long LBO crystal that operated at a temperature of 147.5° C, generating 12 W of 532 nm green light via non-critically phase-matched SHG. The green light was recollimated and steered by two dichroic mirrors for disposing of waste 1064 nm light, and a half-wave plate was used to vertically polarise the green. To reduce the effects of walk-off for the SHG of 266 nm light from green in BBO, the green was brought to a horizontal line focus using 25 and 5 cm cylindrical lenses inside a 5 mm long BBO crystal that was cut and coated for the 532 → 266 nm single-pass process. Similarly, two dichroic mirrors were used to dump the green after a second set of cylindrical lenses used to reformat the beam before it is focused into the Ce:LiCAF oscillator crystal by a 5 cm spherical lens. A wave-plate and polariser were used to control the 266 nm power.

3.3 Ce:LiCAF oscillator

Three highly reflective (>99.5% reflectivity) HR mirrors comprise the 13° folded cerium cavity, which was previously designed for a low lasing threshold and astigmatic compensation. These include a 100 mm radius of curvature (ROC) dichroic mirror and a 50 mm ROC HR separated by approximately 102 mm. The flat high reflecting end mirror was placed on a translation stage to provide a variable cavity length that defines the mode of operation, CW or pulsed. The potential cavity lengths of the oscillator, as a result of its synchronous pump source, include a multitude of rational harmonics [29]. However, only the first few are of interest for this experiment as it is important to maximise pulse energy for characterisation. These lengths are shown in table 3.1, were achieved by careful positioning of the end mirror.

Parameter	CW	1st harmonic	2nd harmonic	3rd harmonic
Cavity length [cm]	75	190	95	63
Plane-mirror distance [cm]	65	180	85	53

Table 3.1: The rational harmonics that were of interest for this particular experiment.

Despite the previous performance of this laser, there was a considerable amount of time

devoted to the initial alignment due to the complexity of this system. It was necessary to take a methodical approach to this, requiring an alignment laser and cleaning to achieve lasing in CW operation, and later the 3rd harmonic.

Precise alignment of this complex system requires a careful systematic approach that is both reliable and safe. The purpose of the following sections are to outline the maintainence and construction procedures that were learned during this thesis which contributed to the operation of the Ce:LiCAF and Ti:sapphire lasers as well as other optics. This includes the removal of contaminents that may inevitably enter the system and inhibit performance and the alignment tools available for building these high-powered lasers.

Dust and dirt can be a significant issue for consistent laser operation, particularly in the ultraviolet and thus should be constantly minimised in the laboratory environment. Dust may burn to produce finer particulates upon entering a highly intense beam, and deposition on to optics is likely to increase absorption and exacerbate any thermal issues present. Cleaning any optical components prior to adding them to the layout, or inserting them into a mount, is good practice as it can be done quickly and methodically via the drag and wipe method. The standard technique of applying a small quantity of acetone or methanol to optical quality tissue paper, which is slowly dragged across the optic, to remove unwanted dirt and biological material proved inadequate for our demanding application and more firm cleaning protocols were developed to remove all organic residues that would otherwise prevent lasing. In particularly dusty environments, dry cleaning, using a small burst of air, is often more appropriate to avoid depositing more contaminents onto optical components.

The positioning of a laser beam focus is important for efficient lasing and other non-linear processes such as frequency generation. It can be difficult to locate due to the small size and high intensity of light that may ablate material, such as fluorescent cards, inserted into the beam path. A knife-edge or razor blade can serve as a precise locater of any focused beam when the edge is brought slowly into the beam. With a power meter, this technique can also be used to asses the power distribution of a beam and ensure its intended propagation.

The focal shape is a particularly important aspect of laser construction that is more crucial in systems where a laser beam is manipulated by asymmetric optics such as cylindrical lenses for producing a line focus in this case. Adjustments are required to ensure that the spot shape returns to a Gaussian after passing through these optics so that later focusing yields a mostly circular spot shape. To check this, focus can be imaged using a high NA lens, and propagated

over several metres. The aim is to ensure that the beam is still collimated in the far-field and is Gaussian in profile which maximises the efficiency of optical pumping and frequency generation.

Cavity ring-down method using a secondary laser

Laser alignment can be very challenging initially, particularly if working with UV light that is absorbed and scattered more readily than visible light, and whose short wavelength demands high quality optics. An alignment laser, which should be of the same wavelength as the test laser, is a tool that can be used for coarse cavity alignment by eye, or using a cavity-ring down (CRD) method. The purpose of the CRD method was initially for measuring losses from propagation in an optical cavity. This information is useful in laser construction for calculating pump thresholds by determining the round trip loss. More practically, it is used as a tool to optimise the cavity in real-time.

The alignment laser is first aligned to the pump laser, by removing the last cavity mirror. It is necessary that the spot sizes of each beam are equal so that the ring-down pulse closely matches the test laser cavity mode with minimal loss. The mirror is then replaced and the CRD laser's back reflection on this mirror is aligned with its incoming beam to cause the back reflection of the pump beam to return to the crystal. A PMT is used to detect the light leakage of the alignment pulse as it resonates in the cavity and determine the round trip losses. It is necessary that the alignment laser is pulsed with a decay time significantly longer than the test laser round trip time and a significantly lower repetition rate than the test cavity to allow the inserted pulse to resonate and decay before the next is inserted.

The losses are calculated by analysing the decay of the pulses that are inserted, specifically their peak intensities. Equation 3.1 describes this relationship, where t_{rt} is the round trip time, τ is the decay time of the intensity peaks, L_0 is the intensity of the first peak while L describes the decaying peak intensities.

$$L = L_0(1 - e^{-t_{\mathrm{rt}}/\tau}) \tag{3.1}$$

Figure 3.1 shows a cavity ringdown of the Ce:LiCAF laser used in this experiment, with a round trip loss of 2.5% caused by three 99.5% HR cavity mirrors and the gain medium itself. The alignment laser was used in returning the oscillator to its original operation if it became misaligned, and to check that the cavity mirrors were not contaminated in any way.

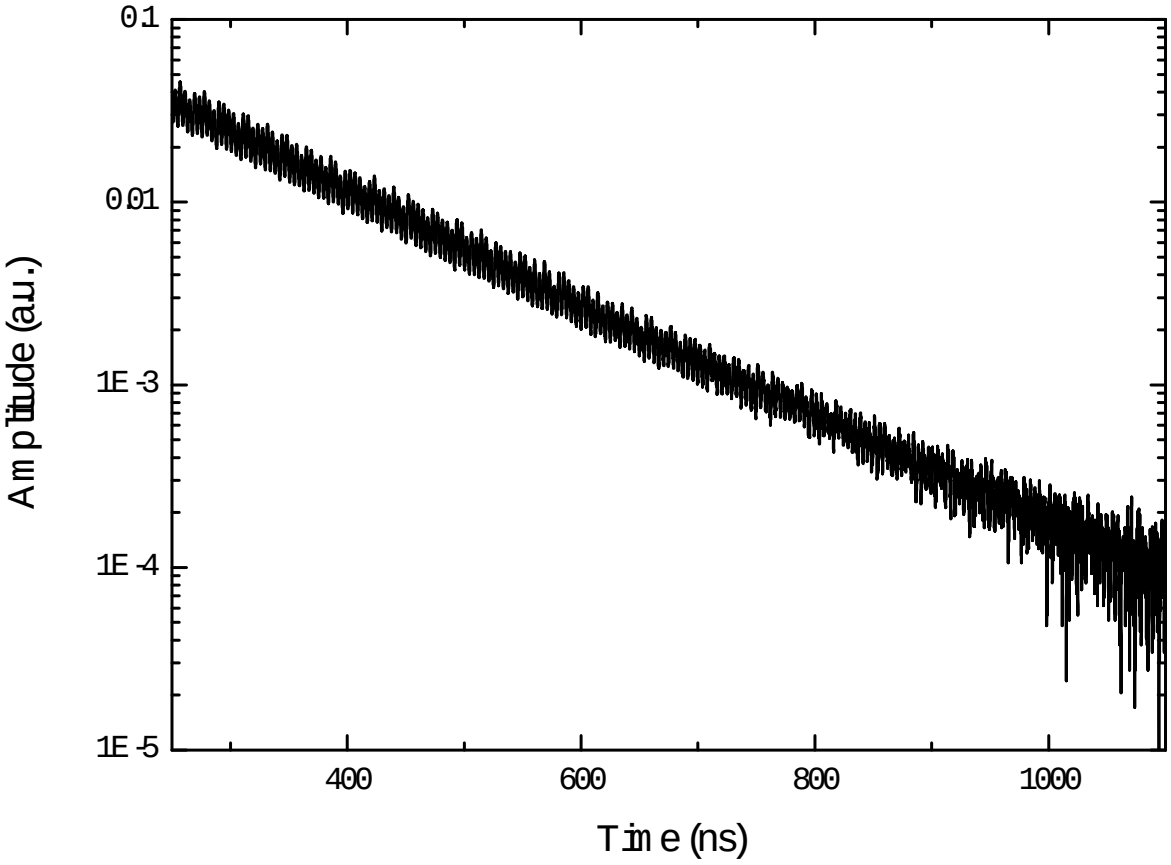

Figure 3.2: A CRD of the mode-locked Ce:LiCAF laser measuring a round-trip loss of roughly 2.5%. The cavity round trip time was approximately 5 ns, with 1 ns alignment pulses.

3.4 Balanced synchronisation

This section describes the procedure that was necessary in constructing the KLM Ti:sapphire oscillator, and balanced synchronisation stage that controls its cavity length. The Ti:sapphire laser (femtosecond design) was mostly pre-built into a single block, with the external addition of chirped mirrors and output coupler. The Verdi V-10 pump source and Ti:sapphire were first placed onto the table for the connection of water cooling pipes. The pump was aligned into the Ti:sapphire with a periscope and two turning mirrors, providing a horizontally polarised pump of 4-6 W. CW output powers of over 800 mW were achieved for pumping at 6 W, but such high powers were not necessary for, and detract from, mode-locked operation. The laser is shown in the left of figure 3.3, while the balanced synchronisation stage is on the right.

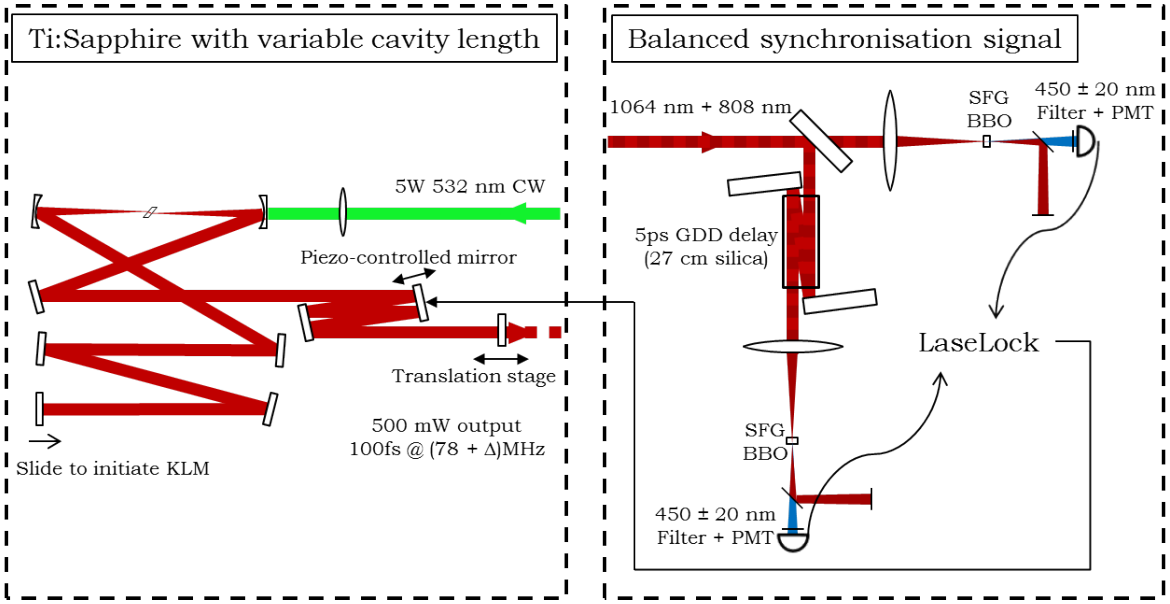

Figure 3.3: Feedback loop to match and maintain the cavity length of a 808nm 78MHz TiSapphire with the 1064nm output of a Nd:YVO_4 pump laser.

Some lasers, from which fluorescence can be detected, may be roughly aligned using a portion of broadly radiating light from the gain medium as a marker for where the cavity mode should be. This was performed for the Ti:Sapphire laser in this experiment; aligning two external chirped mirrors and the output coupler. Positioning of mirrors is approximate with this approach as the fluorescence spot is much larger than the cavity mode diameter itself. However, this satisfies coarse cavity alignment and provides a signal to be measured on a photodiode or power meter. The power output of the laser can then be compared to adjustments of the cavity parameters for improved operation. This includes mirror angles, gain medium position and pump focal position, and cavity length for mode-locked operation. Initiation of KLM operation is performed manually by briefly moving the end-most cavity mirror inward to cause a resonating pulse to form. After initial alignment, and practice, the output coupler was mounted onto a translational stage for later cavity length adjustments. The output beam was combined with the residual Nd:YVO_4 output using a dichroic mirror (DM2 in figure 3.1).

The choice of using 532 nm light or the original 1064 nm pump for synchronisation affects the total power provided by SFG, the length of GDD (group delay dispersion) to delay the pulses, and the wavelength of SFG produced. The 532 nm beam was initially tested but suffered heavily from low signal to noise due to a combination of poor responsitivity from

most detectors at the generated wavelength of 320 nm, and the quality of filters available. Only 300 mW of green light was available for this process in the form of leakage from the 1064/532 dichroic turning mirror, in comparison to several Watts of infrared radiation that would otherwise have been dumped. The phase matching conditions for this initial set up are shown in table 3.2.

Parameter	808 nm (o)	532 nm (o)	320.8 nm (e)
Walkoff [mrad]	0.00	0.00	78.81
Phase velocities [c/]	1.660	1.674	1.668
Group velocities [c/]	1.684	1.722	1.806
GDD [fs^2/mm]	73.9	136.0	289.5
θ [°]	36.4		
d_{eff} [pm/V]	1.95		
Angle tolerance [mrad · cm]	0.24		
Temperature range [K · cm]	10.83		
Mix accep. angle [mrad · cm]	0.62	0.40	
Mix accep. bandwidth [cm^{-1}· cm]	8.19	11.87	

Table 3.2: The type 1 phase-matching parameters for sum-frequency mixing of Ti:sapphire and Nd:YVO4 second harmonic from SNLO nonlinear optics code available from A. V. Smith, AS-Photonics, Alburquerque, NM.

To align the synchronisation stage, the two laser beams are first made collinear by adjusting the two turning mirrors prior to combination, shown in figure 3.1. A $f = 5$ cm achromatic lens was then used to focus the two beams into two 0.1 mm BBO crystals cut at of 40.5°. These were originally purchased for DFG between the 290 nm and 808 nm Ti:sapphire, but were the only crystals readily available with sufficient geometry to accommodate sum-frequency generation at 25.5°.

Due to challenges detecting the signals that were produced, photomultiplier tubes (PMTs) were implemented in addition to band-pass filters (FB400-40) at $\lambda = 450, \Delta\lambda = 20$ nm. The two PMTs that were used initially are shown in figure 3.4, as they were readily available. Both have significant as well as variable gain over the spectral range for any sum-frequency generation. A second H10721-110 PMT was purchased later for producing a more balanced signal.

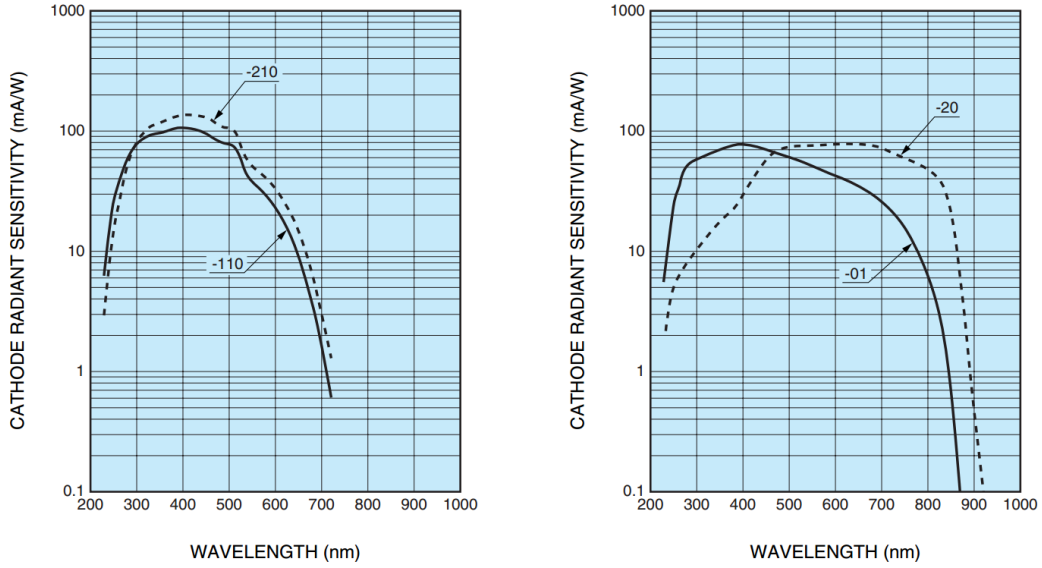

Figure 3.4: The sensitivity curves of the two types of PMTs used in this experiment; Hamamatsu H10721-110 (left) and H10721-20 (right).

Transitioning from using 532 nm to 1064 nm light in this SFG setup allowed for significantly higher signal to be generated, with the added advantage of a more receptive wavelength of 459 nm. The phase-matching conditions for this are shown in figure 3.3.

Parameter	1064 nm (o)	808 nm (o)	459.2 nm (e)
Walkoff [mrad]	0.00	0.00	61.24
Phase velocities [c/]	1.654	1.660	1.658
Group velocities [c/]	1.674	1.684	1.719
GDD [fs^2/mm]	44.0	73.9	158.6
θ [°]	25.5		
d_{eff} [pm/V]	2.02		
Angle tolerance [mrad · cm]	0.45		
Temperature range [K · cm]	28.77		
Mix accep. angle [mrad · cm]	1.05	0.79	
Mix accep. bandwidth [cm^{-1}· cm]	22.36	28.82	

Table 3.3: The type 1 phase-matching parameters for sum-frequency mixing of Nd:YVO4 and Ti:sapphire lasers from SNLO.

3.4.1 Layout and signal balance

Active synchronsiation by balanced cross-correlation requires two arms that produce similarly balanced signals. In order to produce a delay dependent error signal, a timing delay is required in one arm of cross-correlation, implemented using a dispersive medium. The calculations for this are presented, with the aim of separating two pulses in time. The group velocity v_g of light propagating inside a material is related to the derivative of frequency ω with respect to material wavenumber $k(\lambda)$ in the form of equation 3.2. Equation 3.3 was used to convert between the physical size d of the dispersive medium delay line and relative timing difference ΔT based on the group velocities of two wavelengths.

$$v_g = \frac{\mathrm{d}\omega}{\mathrm{d}k} = \frac{d}{T} \tag{3.2}$$

$$d = \Delta T \left(\frac{v_{\mathrm{g},2} v_{\mathrm{g},1}}{v_{\mathrm{g},2} - v_{\mathrm{g},1}} \right) \tag{3.3}$$

The timing delay that GVD introduces between the pump and probe (Nd:YVO_4 and Ti:sapphire) should be less than the duration of the longer pulse, in this case the pump, but significant enough to overcome lasing and environment variations that cause noise. The duration of 1064 nm pulses is approximately 28 ps, of which the timing delay should be a reasonable fraction to minimise noise whilst providing sufficient signal.

Silica is a commonly available material with a moderate amount of dispersion that was conveniently available in the lab. The delay line is constructed from three 3 cm long cylinders and two mirrors for a triple-pass through the 9 cm of silica for a total of 27 cm. This value was then used to determine the relative timing difference of 4.7 ps after propagation through the delay line. The potential issues of synchronisation using this configuration include Fresnel losses and significant broadening of individual pulses. Both of these may imbalance the two synchronisation arms, which is dealt with by variable the gain voltage supplied to the PMTs.

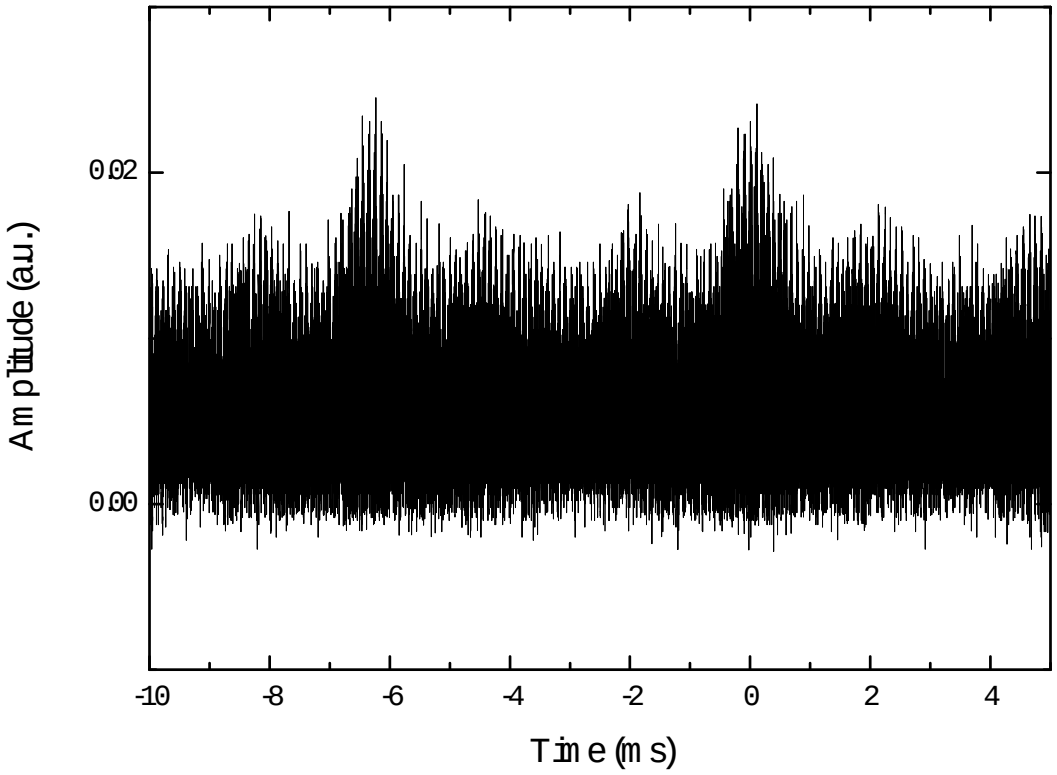

Figure 3.5: Cross-correlation of asychronously pulsed Ti:sapphire and Nd:YVO4 lasers that produces a beat frequency, initially detected using a PMT for optimisation of alignment.

3.4.2 Synchronisation and modeling

Assessing the precision of synchronisation is an important step to validating its use in a XFROG system, as timing variations will detract from synchronised characterisation. Initial investigations were performed by adjusting the Nd:YVO_4 and Ti:sapphire lasers to produce a steady beat signal. A clean sweep of the error signal at a constant frequency offset Δf between the two lasers describes the feedback response that is interpreted by the LaseLock system. This is multiplied by a factor of $\Delta f / f_0$ to return to the original pulse timing, as discussed in chapter 2. This is shown in figure 3.6 with the timing of the x-axis adjusted by $\Delta f / f_0$.

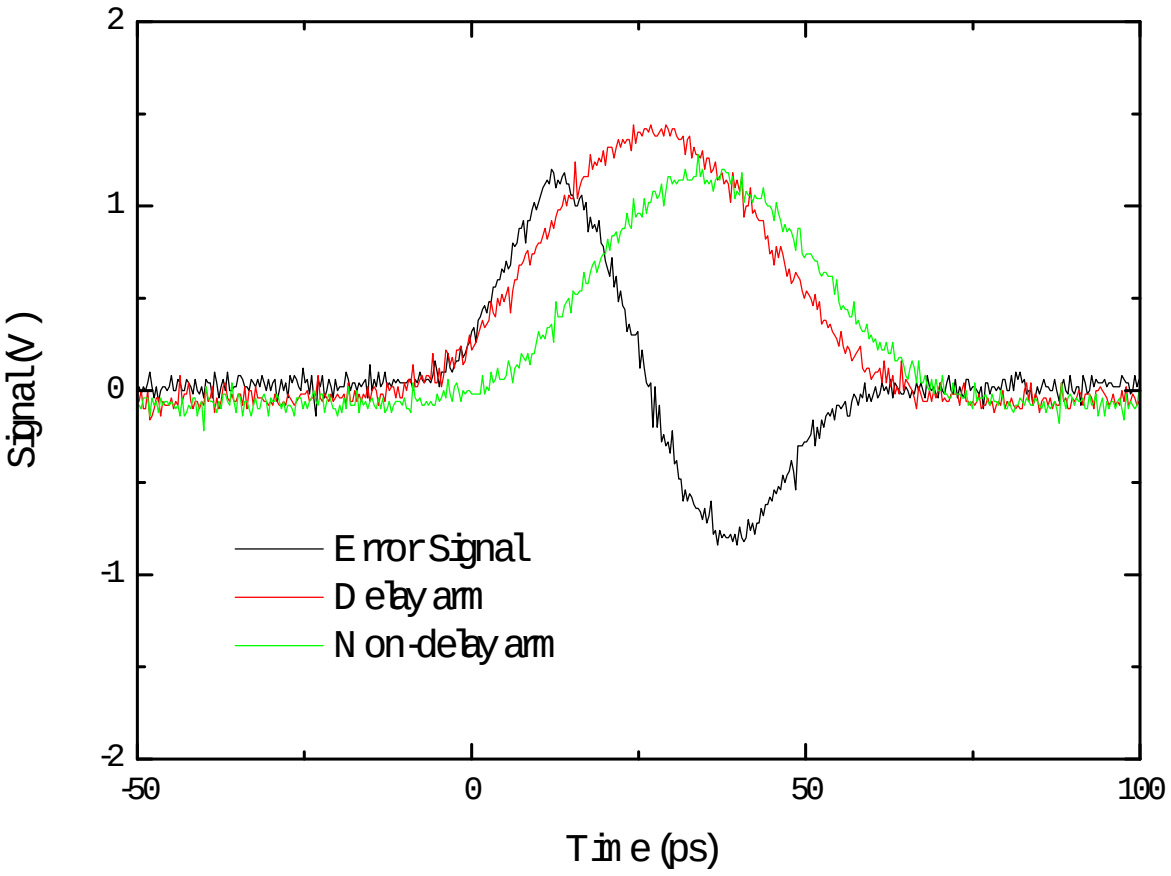

Figure 3.6: Cross-correlation and error signal provided to LaseLock, recorded at a frequency mismatch of 245 Hz.

Modeling of the shape in figure 3.6 is shown in figure 3.7 using voltages that were recorded in the case of a successful synchronisation. The purpose of this reconstruction was to provide an estimation of how the timing fluctuates between the two pulse trains. To this end, the centre gradient of 0.55 V/ps was used to estimate timing jitter associated with the system.

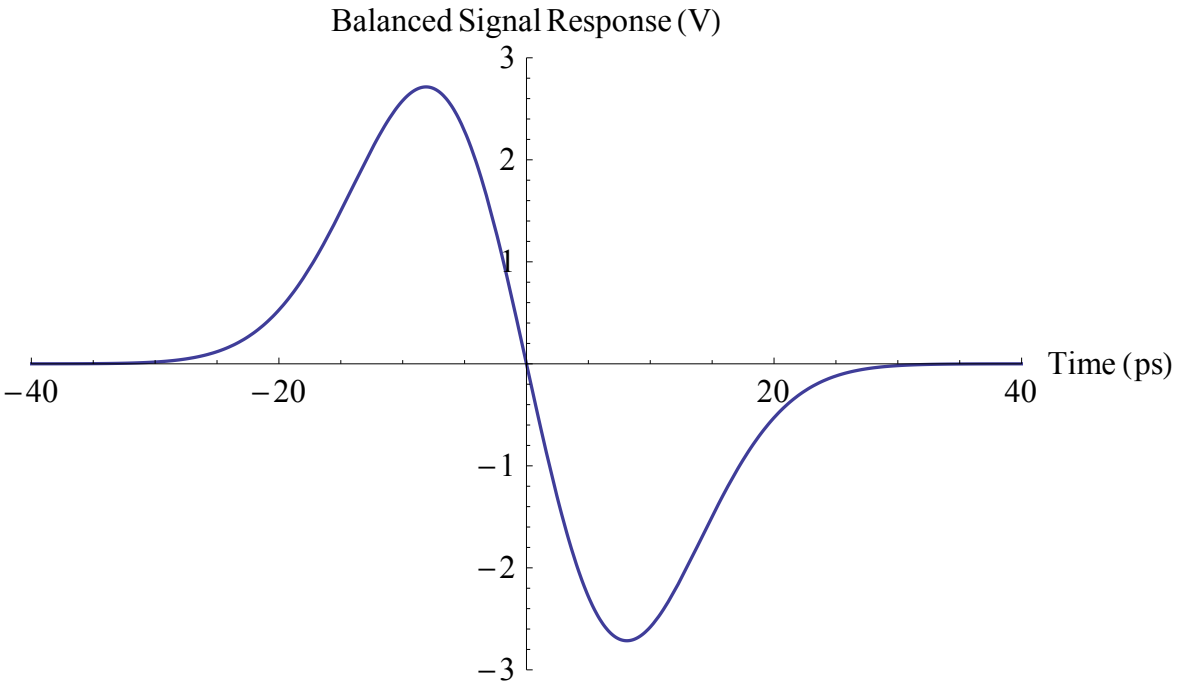

Figure 3.7: Modeling of error signal to provide a means of quantifying the timing jitter. The gradient of this model is 0.55 V/ps, which was used to convert error signal and two synchronisation signals from voltage to time.

From this model, the timing jitter of the error signal and each synchronisation arm was constructed based on the variation in error signal voltage. This is discussed in chapter 4.

3.4.3 LaseLock feedback control

Signal processing was performed using a LaseLock PID controller. This system has several settings for balancing and scaling the error signal to useable signal levels. Since we are using variable gain PMTs, the cross-correlation signal was adjusted to achieve roughly 1V maximum prior to insertion into the controller. The signal for synchronisation itself relies on PID settings; these provide a proportional, integrated, and differential response to the provided error signal. After producing a clean error signal, the careful adjustment of these values was necessary to achieve synchronisation. Fine-tuning of the response to reduce fluctuations is performable only when the system is synchronised.

3.5 Frequency resolved optical gating

A Mesa-Photonics commercial FROG system was set-up temporarily in place of the XFROG (also Mesa-Photonics) for characterising the Ti:sapphire pulse and to practice alignment. The inserted beam was split into fixed and variable delay lines that sweep the pulses through one another in time. Ideally, both the FROG and XFROG systems are implemented simultaneously for the real-time deconvolution necessary for XFROG, but only one suitable spectrometer was available, hence the temporary placement.

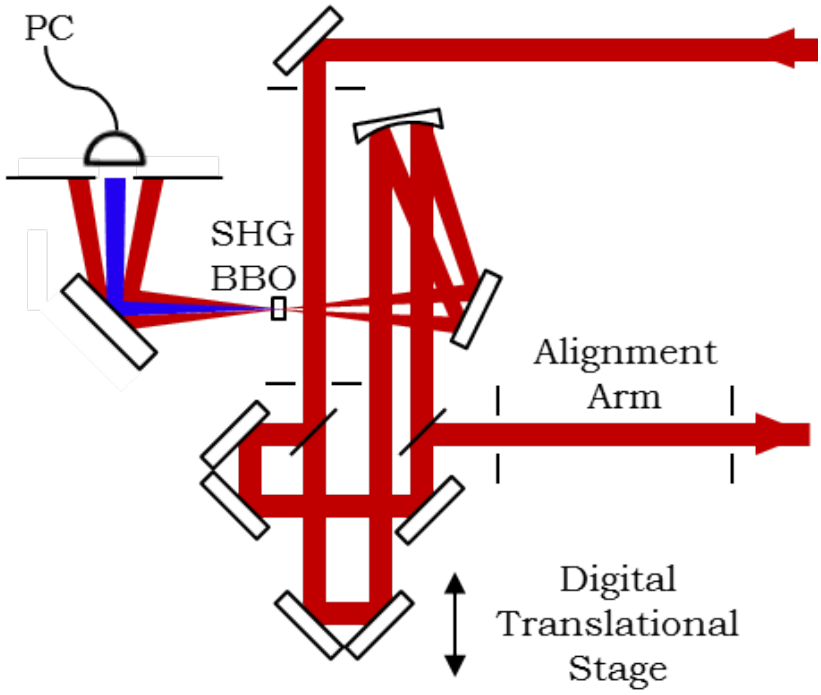

Figure 3.8: FROG layout for the characterisation of the Ti:Sapphire via second harmonic generation to provide a calibrated measurement that is then used in the X-FROG system.

The phase matching conditions for this process are outlined in table 3.4, satisfied by the thin-crystal BBO crystal included in the commercial system.

Parameter	808 nm (o)	808 nm (o)	404 nm (e)
Walkoff [mrad]	0.00	0.00	67.55
Phase velocities [c/]	1.660	1.660	1.660
Group velocities [c/]	1.684	1.684	1.740
GDD [fs^2/mm]	73.9	73.9	192.8
θ [°]	28.9		
d_{eff} [pm/V]	2.00		
Angle tolerance [mrad · cm]	0.36		
Temperature range [K · cm]	20.15		
Mix accep. angle [mrad · cm]	0.72	0.72	
Mix accep. bandwidth [cm^{-1}· cm]	17.70	17.70	

Table 3.4: The type 1 phase-matching parameters for second harmonic generation of Ti:sapphire.

3.5.1 Overlapping two beams for X-FROG

Aligning the input beams of the Mesaphotonics X-FROG system requires spatial as well as timing overlap. The non-linear crystal in this system is only 500 μm thick, so careful adjustments are necessary to obtain a useable signal from the cross correlation of Ti:Sapphire and far weaker cerium ones. The temporal offset that arises due to path length differences between the synchronisation module and the X-FROG module is corrected for with a delay line in the path of the Ti:S probe laser. Due to the low power provided by the cerium, it is necessary to minimise UV reflection losses from mirrors that would otherwise detract from the 452 nm DFG (290 nm - 808 nm) signal.

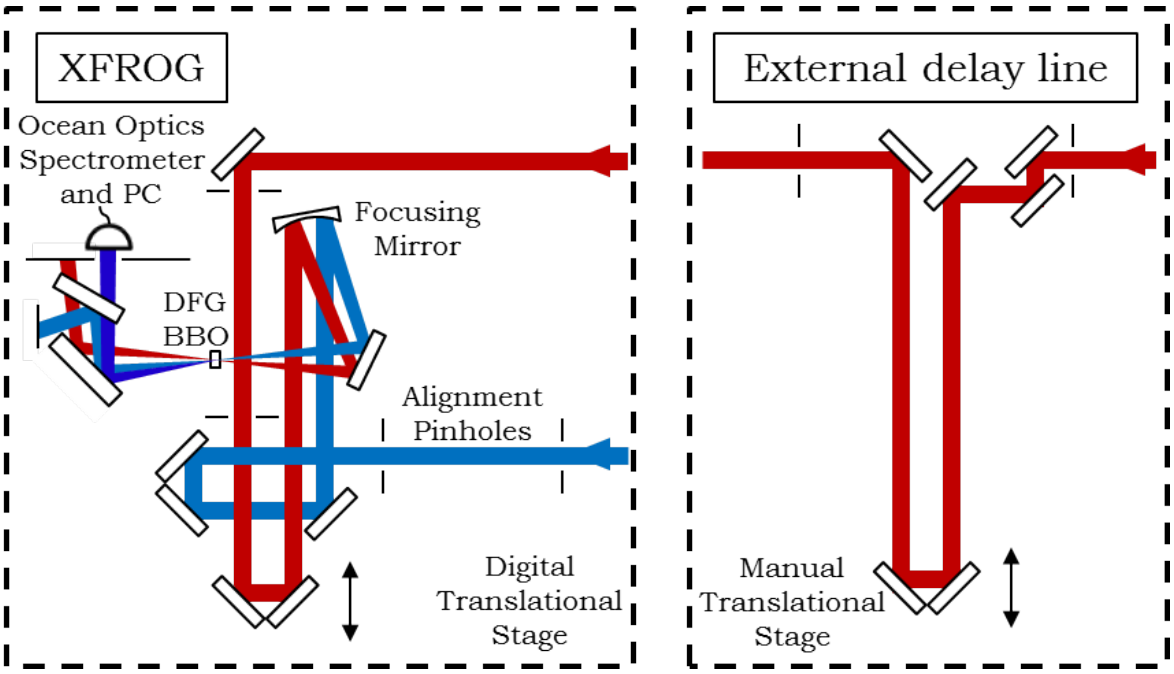

Figure 3.9: X-FROG layout for characterising DUV pulses via difference frequency generation with a 100fs Ti:Sapphire probe laser.

By replacing the Brewster output coupler with a 266 nm HR mirror, initial DFG results can be acquired with the significantly more powerful 266 nm pump without the cerium laser operating. This is a helpful stepping stone as the geometry and timing of this arrangement is closely analogous to the intended design of figure 3.1. This approach also bypasses issues related to low signal, particularly in aligning the two beams and correcting for timing offset simultaneously. The phase matching conditions necessary for both DFG process are included in tables 3.5 and 3.6

Parameter	808 nm (o)	396.5 nm (o)	266 nm (e)
Walkoff [mrad]	0.00	0.00	86.53
Phase velocities [c/]	1.660	1.694	1.683
Group velocities [c/]	1.684	1.785	1.908
GDD [fs^2/mm]	73.9	218.5	440.3
θ [°]	44.3		
d_{eff} [pm/V]	1.87		
Angle tolerance [mrad · cm]	0.18		
Temperature range [K · cm]	6.66		
Mix accep. angle [mrad · cm]	0.56	0.27	
Mix accep. bandwidth [cm^{-1}· cm]	4.47	8.15	

Table 3.5: The type 1 phase-matching parameters for difference-frequency mixing of Ti:sapphire and Nd:YVO4 fourth harmonic.

Parameter	808 nm (o)	452.4 nm (o)	290 nm (e)
Walkoff [mrad]	0.00	0.00	83.29
Phase velocities [c/]	1.660	1.683	1.675
Group velocities [c/]	1.684	1.751	1.853
GDD [fs^2/mm]	73.9	174.7	358.1
θ [°]	40.4		
d_{eff} [pm/V]	1.91		
Angle tolerance [mrad · cm]	0.21		
Temperature range [K · cm]	8.32		
Mix accep. angle [mrad · cm]	0.58	0.32	
Mix accep. bandwidth [cm^{-1}· cm]	5.92	9.78	

Table 3.6: The type 1 phase-matching parameters for difference-frequency mixing of Ti:sapphire and Ce:LiCAF.

When the two lasers are only just asynchronous in their repitition rates, the beat frequency of the two pulse trains will slowly pulse to result in a varying SFG/DFG signal. Applying similar methods of aligning the balanced synchronisation module, the SFG of a single

synchronisation arm, or the error signal itself was compared to the DFG produced by mixing the 266 nm pump light with 808 nm Ti:sapphire light. The resultant light at 396 nm was detected using a bandpass filter 400 $\Delta\lambda$ = 40 nm, after which timing corrections shown in figure 3.10 were made.

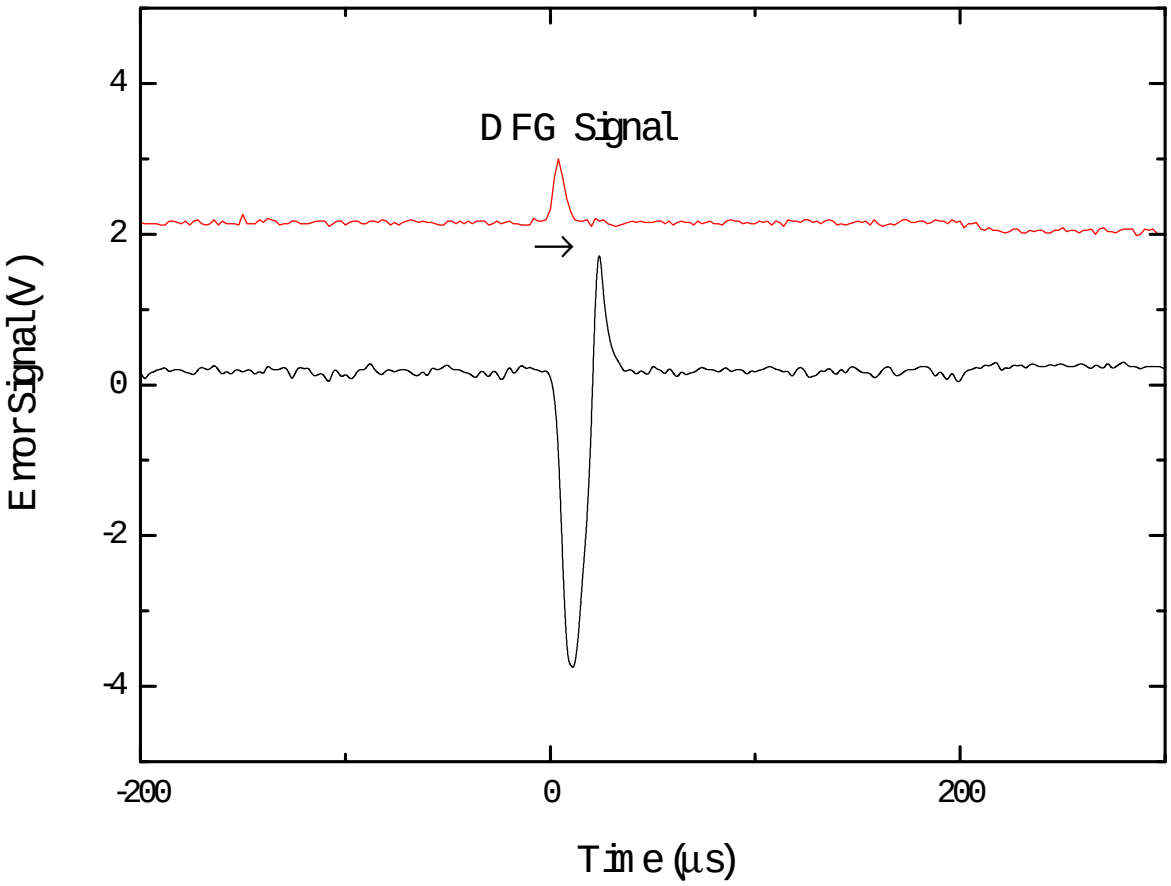

Figure 3.10: Error signal from the balanced synchronisation system and 266 nm - 800 nm DFG signal when approximately aligned in time by adjusting the delay line of the Ti:sapphire.

4

Results and discussion

4.1 Introduction

This section serves to detail the outcome and effectiveness of the apparatus that were constructed via the methods of chapter 3. First the performance of the Ce:LiCAF laser is briefly presented, followed by estimation of the timing error of synchronisation which affects future characterisation, and the preliminary characterisation of the Ti:sapphire probe and 266 nm pump beams in working towards characterising the Ce:LiCAF cavity.

4.2 Ce:LiCAF oscillator

The most challenging aspect of working with the Ce:LiCAF oscillator lies in its pump stage, which was modified by repositioning of the 12:1 chopper cycle. This noticeably increased the thermal effects present in the LBO crystal which was subject to 26 W of 1064 nm radiation, although despite this, pump powers above 12 W in the green were obtained. The threshold

pump power for the Ce:LiCAF cavity is roughly 2.5 W (unchopped) of 266 nm light. After moving the chopper (to allow synchronisation), the 266 nm power was reduced from 3.2 W to approximately 2.5 W. This reduction was most likely due to increased thermal effects in the LBO crystal.

Despite these low pump powers, the Ce:LiCAF cavity could be aligned for CW and 3rd harmonic mode-locked operation, with the intention of moving to the 1st harmonic for maximising pulse energy. The 3-mirror cavity is aligned more easily without the Brewster's plate, which was the only available output coupler, and optimised using the portion of laser light lost on the faces of the Ce:LiCAF gain medium.

In addition to this overall power reduction, stability was reduced, with slow degradation over some weeks to where the cerium laser was below the threshold for lasing. While this caused issue with characterisation of the Ce:LiCAF oscillator, re-examination of these optics is timely and was not within the scope of this project. Given the deteriorating performance of the cerium laser it was decided to focus on the pulse characterisation and synchronisation of the pump laser serving as a proxy for the cerium laser.

4.3 Pulse Characterisation

4.3.1 Frequency-resolved optical gating

Characterisation of UV pulses using X-FROG requires good knowledge of the reference pulses from the Ti:Sapphire laser as a means of calibration to ascertain the pulse features of the Ti:sapphire reference laser. This is necessary to deconvolve the cross-correlation FROG accurately, with both FROG measurements and deconvolution ideally performed simultaneously in real time.

The FROG pulse measurement yielded a FWHM of approximately 80 fs as shown in figure 4.1, which was extracted from a FROG scan shown in 4.3.

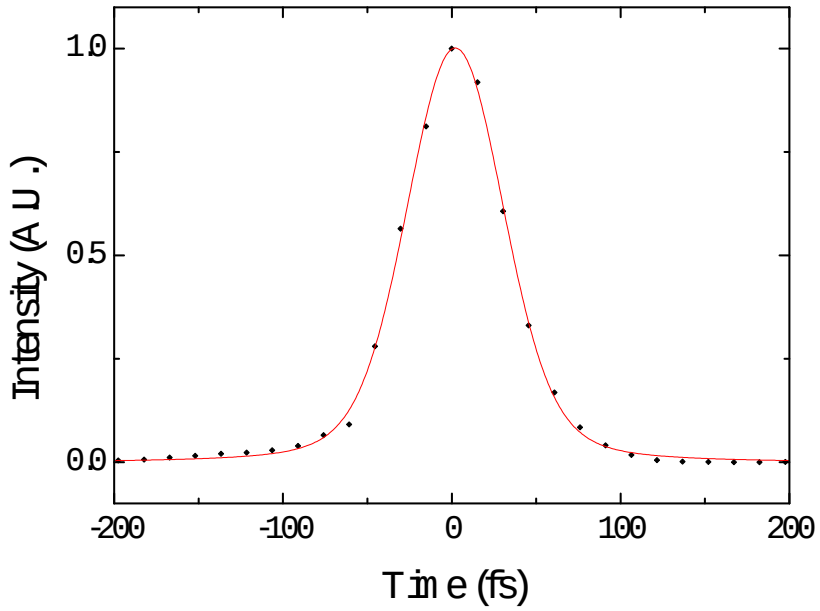

Figure 4.1: Autocorrelation of a Ti:Sapphire pulse with itself to yield a pulse FWHM of 80 fs, extracted from 4.3.

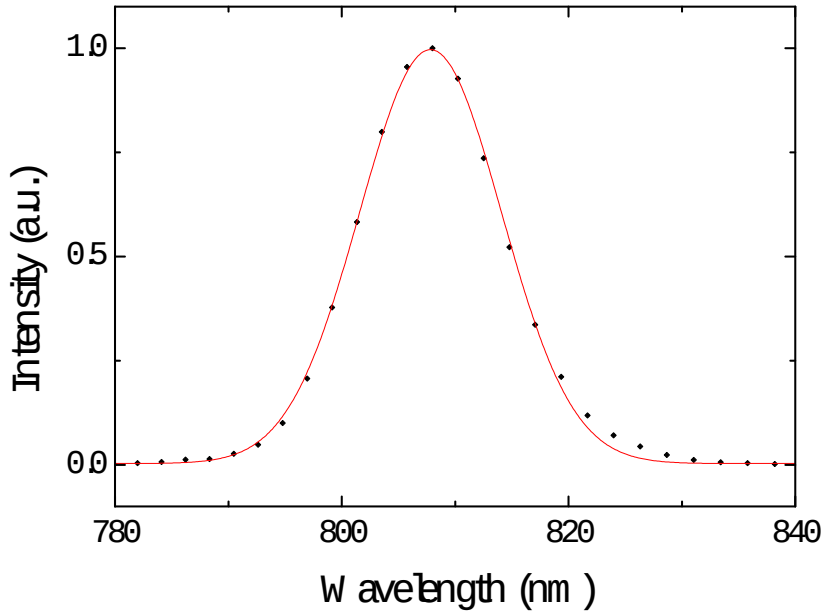

Figure 4.2: Spectrum of Ti:Sapphire pulses detected in the FROG system measuring a central wavelength of 808 nm and a FWHM bandwidth of 15 nm. This is a simplified bandwidth with no time dependence extracted from figure 4.3

The spectrum of the Ti:sapphire is shown in figure 4.2, which shows that the laser was operating with significantly less than the available bandwidth.

A more convenient method displaying this pulse characterisation for the assessment of

chirping is via a FROG trace as shown in figure 4.3. In the case of significant chirping, the trace would more closely resemble a diagonal line [35]. As can be seen here, the FROG trace shape is near-perfect, which implies that the Ti:sapphire pulses are near transform limited albeit also spectrally limited. This 80 fs pulse is much shorter than the 266 nm pump pulses and Ce:LiCAF pulses of which are on the order of picoseconds. This not a hindrance on any later characterisation, which may actually benefit from a longer test pulse with a narrower bandwidth.

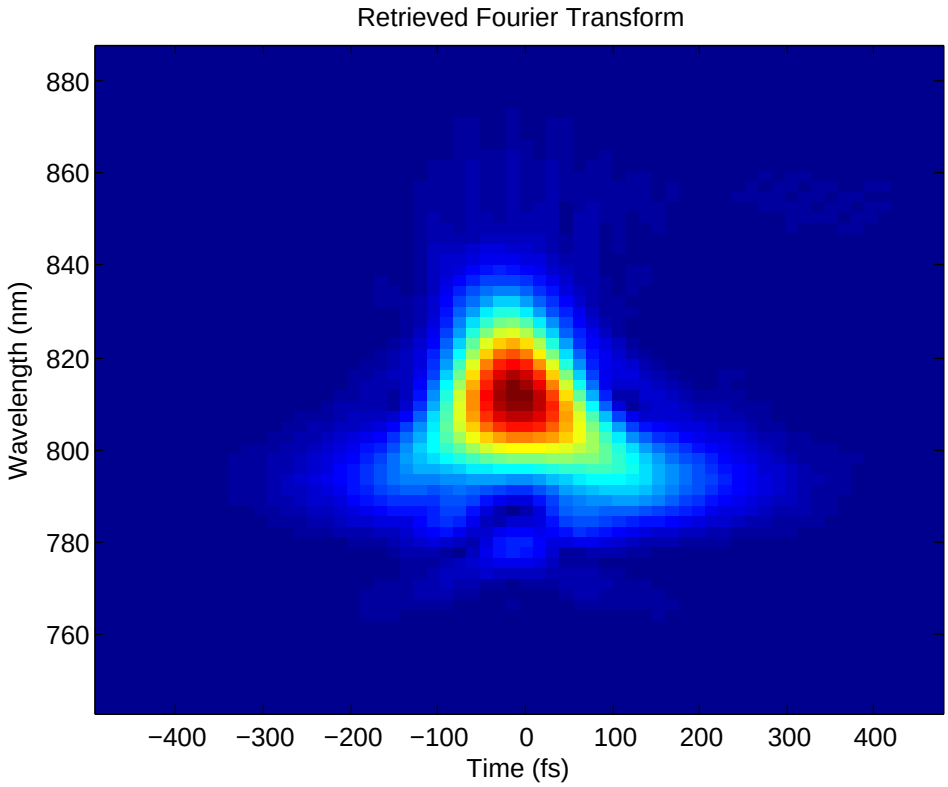

Figure 4.3: FROG trace of a Ti:Sapphire pulse with itself at a resolution of 64 by 64 pixels.

4.3.2 Overlapping two beams for X-FROG

In order to establish an effective pathway to characterising the 290 nm Ce:LiCAF oscillator, the 266 nm pump was first selected as a high powered alternative to make alignment easier. The process of aligning the 266 nm and 808 nm pulse trains included the use of asynchronous sampling described in chapter 3. An asynchronous cross correlation trace was recorded as shown in figure 4.4 and the pulse duration of the 266 nm pump was measured to be on the order of 20 ps.

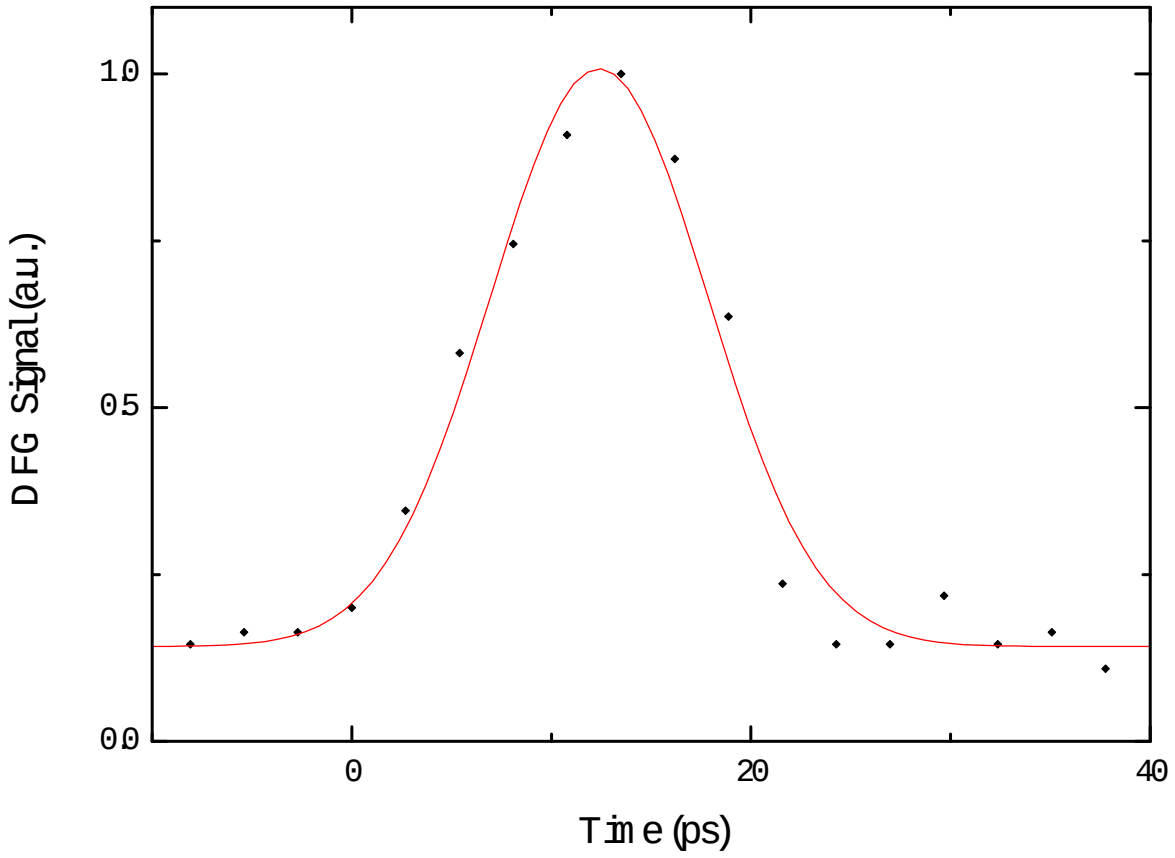

Figure 4.4: Asynchronous cross-correlation of 808 and 266 nm light for alignment purposes, effectively measuring the 266 nm pulse duration of approximately 13 ps.

With this configuration, the synchronisation was activated, and a spectrum of the DFG cross-correlation was recorded using a Ocean Optics 2000+ spectrometer in the range of 320 - 500 nm. This is shown in figure 4.5, and closely matches the expected wavelength of 396.5 nm. The approximately 13 ps 266 nm pulses do not have sufficient spectral bandwidth (only just resolved by the spectrometer) to allow meaningful X-FROG measurements of the pump laser. However, we have validated this approach for characterising deep UV ultrafast pulses. Note that the bandwidth of the cerium laser was typically of order 5 nm and thus *would* be resolvable using this X-FROG system.

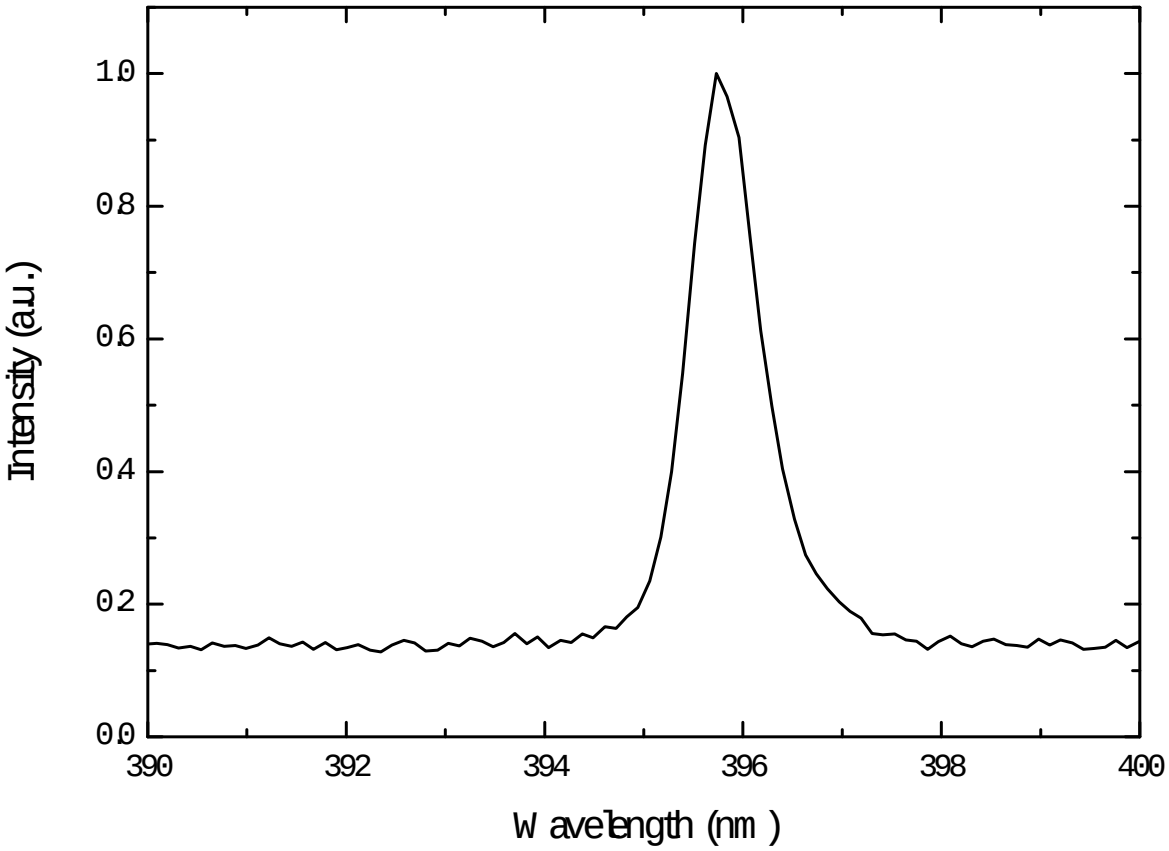

Figure 4.5: Synchronous cross-correlation of 808 and 266 nm light, which was inserted into a spectrometer, measuring a DFG wavelength of 396 nm.

4.4 Active synchronisation

Active synchronisation of the 266 nm pump arm and Ti:sapphire probe laser was successful. This section describes the synchronisation results including determination of timing jitter and stability.

The synchronisation performed here required that the frequency of the Ti:sapphire oscillator was as close as possible to the pump laser. A manual delay line supporting the Ti:sapphire output coupler, in addition to manual offsets of the piezo-mounted cavity mirror enabled this. However, once closed, the feedback loop does not immediately synchronise via the first error signal encountered. Careful adjustment in an open configuration is useful for matching the cavity lengths as close as possible which makes the cross-correlation pulse longer. A voltage ramp is supplied to the piezo-mounted mirror, which scans the cavity length very slowly. This then synchronises to a sufficiently slow cross-correlation peak, but can take several seconds to take effect. The ramp and subsequent synchronisation is shown in figure 4.6

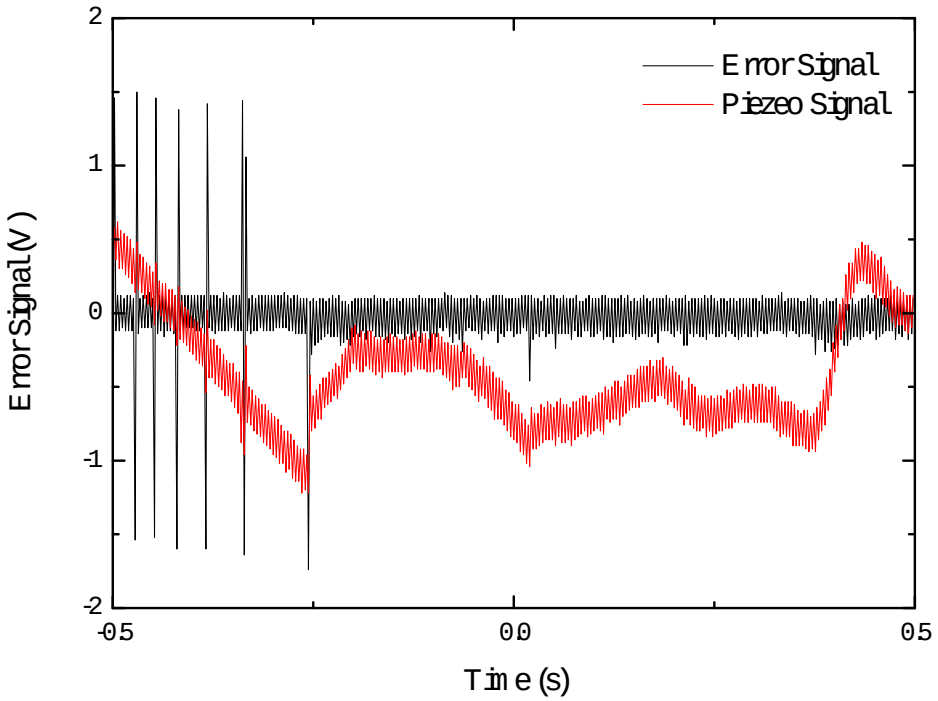

Figure 4.6: Piezo ramping voltage and error signal indicating the process of synchronisation to a balanced cross-correlated error signal. These traces were recorded with an oscilloscope set to peak detect, hence the apparent high frequency noise is in fact an envelope of the noise signal.

4.4.1 Time uncertainty analysis

During the synchronisation of the Ti:sapphire and Nd:YVO_4, the error signal and precision of synchronisation fluctuate in time. The nature of these timing variations can be classified by the scale on which they occur; unavoidable fast variations that describe timing error, and undesirable slow variations that are more likely to unlock synchronisation.

The modeled error signal in chapter 3 provided a conversion from error signal voltage to timing offset, for estimating the time error of this synchronisation system. Figure 4.7 shows the errors that were recorded using unbalanced detectors, although as variable gain was used, this was not a significant issue.

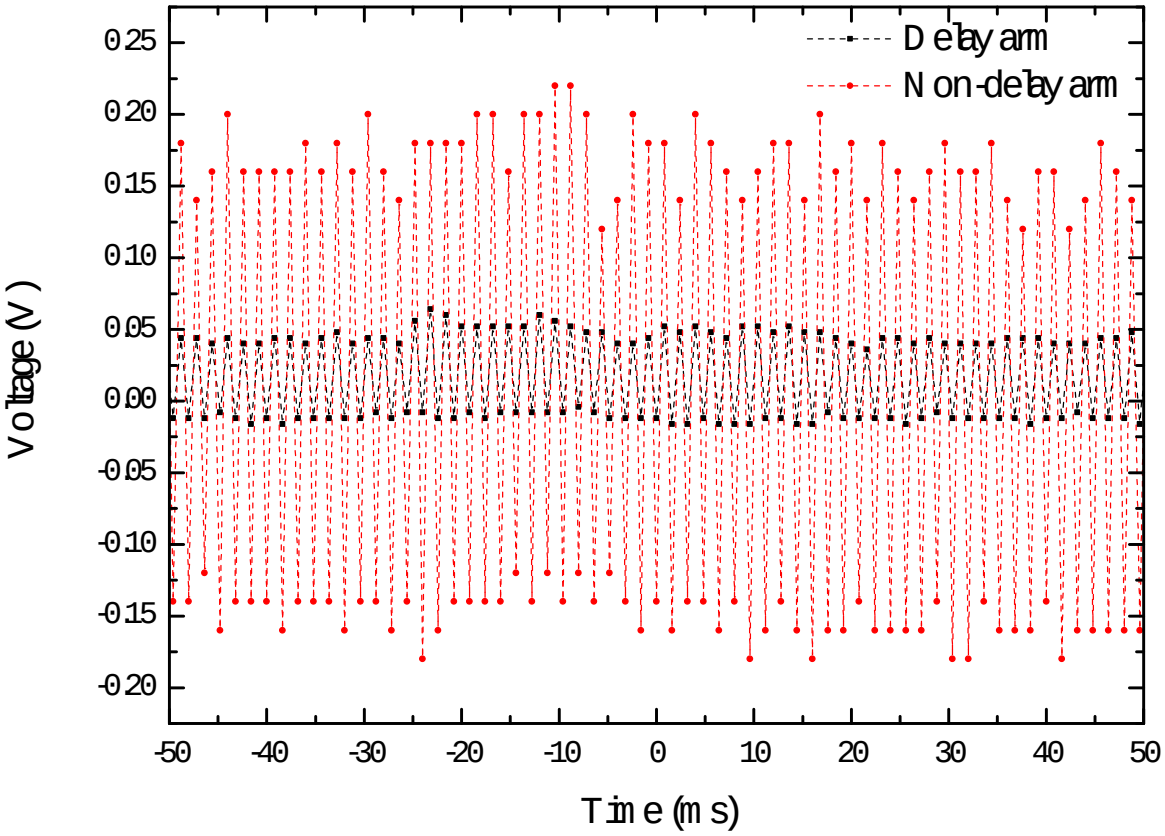

Figure 4.7: Pulse timing error between the two arms of synchronisation, displayed as a voltage, to indicate that the system is imbalanced. These traces were recorded with an oscilloscope set to peak detect, hence the apparent high frequency noise is in fact an envelope of the noise signal.

Despite the imperfect balance between the arms, synchronisation was achieved with the two different PMTs discussed in chapter 3. This is shown in figure 4.8 in terms of a recorded error signal that was converted from voltage to the temporal domain using the modeled error

signal's gradient of 0.55 V/ps. The root mean square (RMS) of the timing errors in this arrangement was calculated to be 45 fs, and so this synchronisation provides no better than 100 fs of precision.

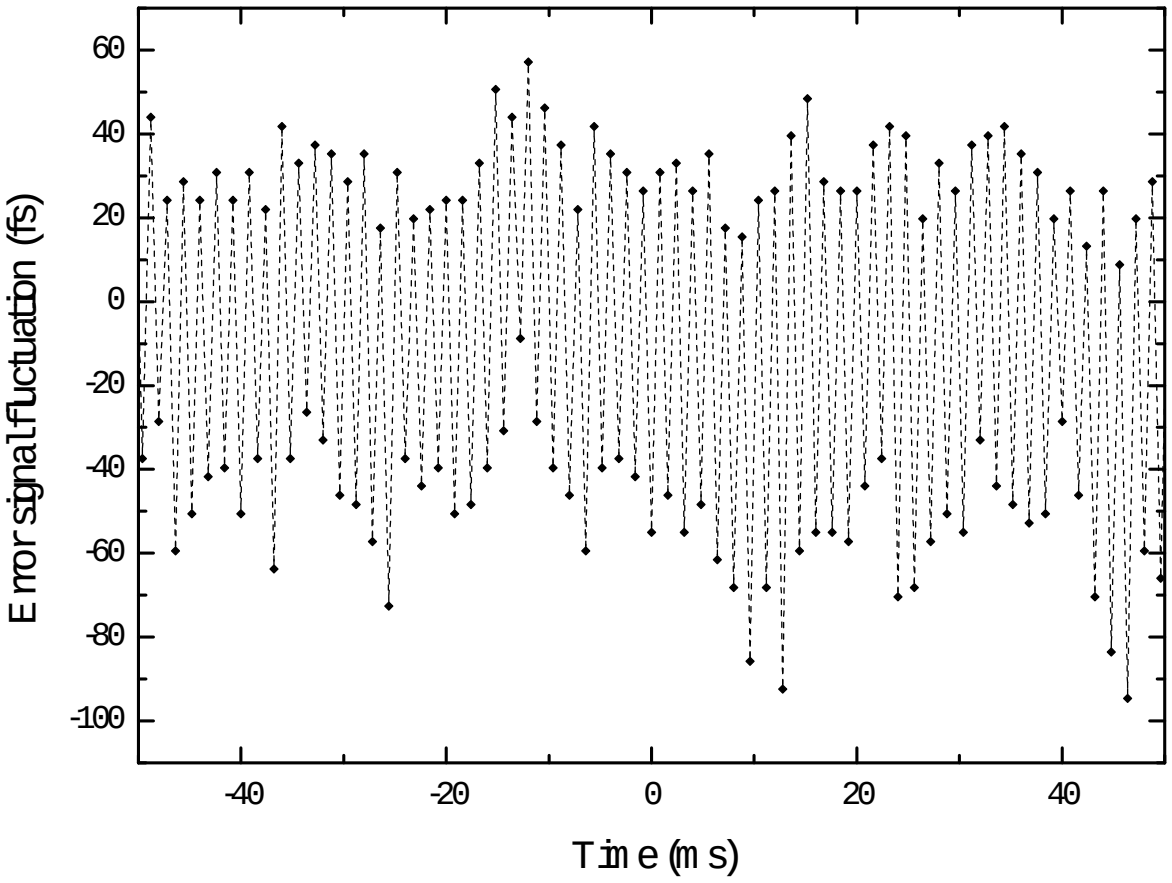

Figure 4.8: Fluctuation of the error signal used for balanced synchronisation converted to a time error using a modeled gradient of 0.55 V/ps. This trace was recorded with an oscilloscope set to peak detect, hence the apparent high frequency noise is in fact an envelope of the noise signal.

While the above result is adequate for the characterisation of the Ce:LiCAF's 6 ps pulse duration, it will become increasingly worse as the test pulse is compressed; the effort to reduce timing uncertainties is important. After purchasing a second PMT for balance, and blocking much light leakage into the system, synchronisation was improved. While the asymmetry in voltage response between the two remained present, the timing errors were significantly improved.

Figure 4.9 shows the timing uncertainty together with the choped green (532 nm) and the difference frequency signal (266 nm - 808 nm). This data was recorded during relatively stable

operation of the synchronisation stage. A third PMT (H10721-20) was used for sampling the difference frequency generation between 266 nm and 808 nm light. Although there is notable slow variation in the error signal, the RMS timing uncertainty *during* cross-correlation was calculated to have a value of approximately 10 fs. The validity of this duration is supported by the similarity between the 532 nm chopped signal and DFG between its second harmonic and the Ti:sapphire probe.

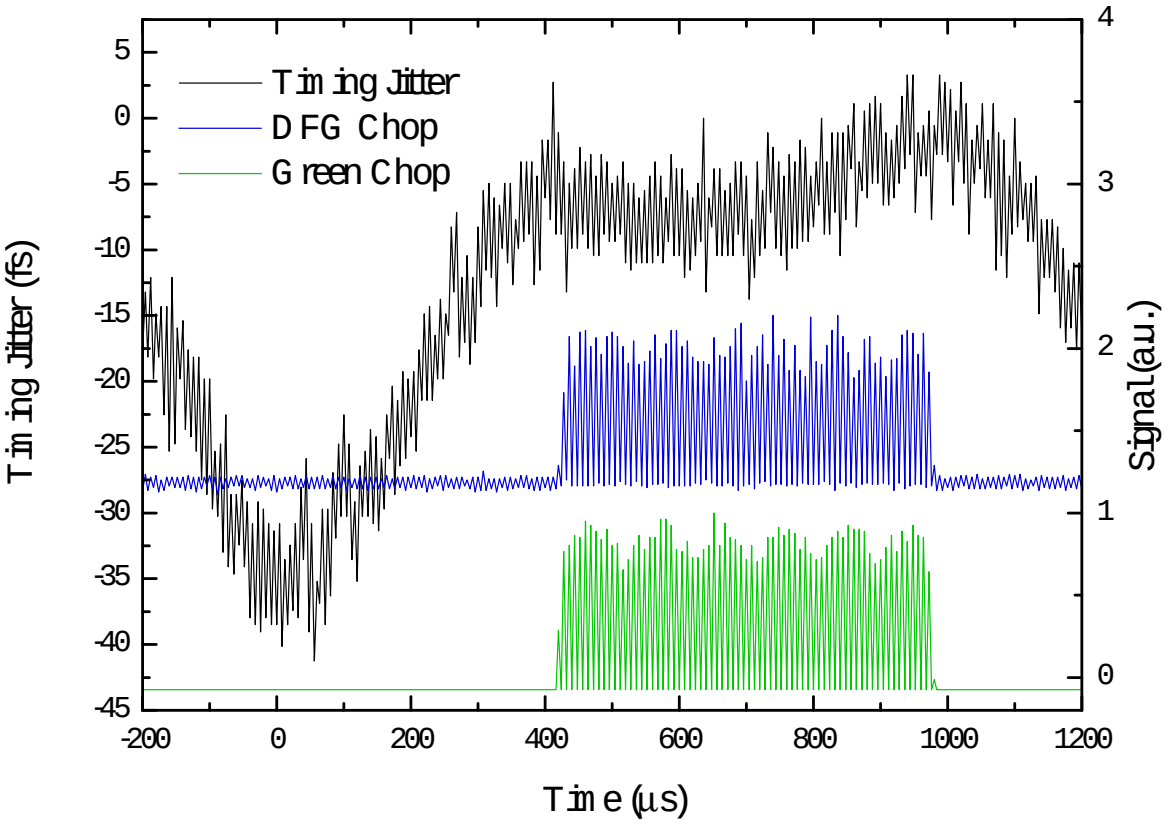

Figure 4.9: Timing jitter of the error signal used for balanced synchronisation whilst the DFG of cross-correlation between 266 nm and 808 nm was recorded using a PMT. The RMS timing error was calculated to be 10 fs for the duration of the open chopper cycle.

The modulation of the green and DFG signals is the result of aliasing by the the oscilloscope that was available. During the open duty cycle, there are approximately 50 000 pulses, yet only a few hundred are sufficient for X-FROG techniques. This work therefore shows that the Ti:sapphire laser pulses could be locked to be synchronous with the Nd:YVO_4 pulses with sufficient precision to perform X-FROG measurements for pulse characterisation.

Order, entropy

Life; *loves to learn, learns to love*

Time is relative

A haiku by Adam Sharp

5

Conclusion

The purpose of this work is synchronous characterisation for working towards the construction of a KLM Ce:LiCAF laser as a robust femtosecond DUV source. In the effort to reduce ultrashort pulse durations in the DUV, the characterisation stage is essential. We have demonstrated the synchronisation of the pump source and probe laser in this apparatus, with timing jitter on the order of 10 fs. This will improve upon asynchronous methods of cross-correlation in both temporal uncertainty and sensitivity. In our synchronisation stage's current configuration, the temporal uncertainty achieved during a single chop cycle is sufficiently low that synchronous characterisation of pulses DUV pulses in a X-FROG system is viable. In constrast, the asynchronous characterisation methods presented in [36] had timing jitter from mechanical vibrations affecting with the pump-probe beat frequency, yet were capable of pulse measurements on the order of 50 fs. It is likely that our system would be able to achieve at least this level of accuracy in its current state.

5.1 Limitations and improvement

The ultraviolet region is a challenging one to work with due to high photon energies, short wavelengths. UV light exhibits increased loss from, and degradation of, optical components such as mirrors that is generally unavoidable. There is the necessity for elaborate frequency conversion from longer wavelengths which requires relatively high powers at longer wavelengths, particularly at the original 1064 nm of pump light. While the methods of balanced synchronisation presented here function mostly as intended, thermal effects in the 266 nm generation stage should be dealt with, but were beyond the scope of this work.

While synchronisation is functioning, there is always the potential for improvement. The use of PMTs for synchronisation is not ideal as they are relatively expensive and noisy compared to PDs. The sensitivity of the H10721-110 detector used for synchronisation peaks close to the 460 nm cross-correlation signal, which is desirable. However, due to the repositioning of the chopper discussed in chapter 3, there was a significant amount of waste light being dumped at 532 nm. This wavelength is also well detected, and in combination with small cracks/gaps between the filters and PMTs, produced a detectable background noise albeit minor compared to the SFG signal. The most appropriate solution to these issues is to transition to photodiodes and to carefully enclose the system in a light tight box to reduce signal noise.

In addition to unavoidable timing errors, a misshapen error signal, however minute, can affect the locking voltage for which the system is balanced. This could be the result of asymmetry between the power generated in the two cross-correlation arms, particularly that which contains the silica delay line. In order to provide a significant timing difference between the two arms, a triple-pass through 9 cm of silica was set up (27 cm total), resulting in a 5 ps delay between the 808 nm Ti:Sapphire and 1064 Nd:YVO_4 pulses. The losses caused by Fresnel reflections at these many surfaces could cause an imbalance due to loss, or even contribute to the SFG. It was noted that even CW contribution from the Ti:sapphire laser was detectable. This will ultimately result in increased timing fluctuation. The large amount of material required to separate the two pulses is due to their spectral proximity. However, this thickness will also result in pulse broadening, as second-order dispersion takes effect. This may affect SFG in the delayed arm; a longer pulse duration reduces overall conversion efficiency and may affect signal shape if the pulse distortion is significant enough.

In order to generate a more reliable signal in both arms of active synchronisation, a

different method of pulse delay may also be useful. The centre wavelengths of each source are relatively close, but FROG the measurements of the Ti:Sapphire laser in figure 4.3 indicates that it operates primarily near 808 nm with a bandwidth of roughly 15 nm. This can be advantageous, as it allows for the use of dichroic mirrors to create a physical path length difference, instead of relying on GVD. Dichroic mirrors that are capable of transmitting one set of pulses while reflecting the other are readily available at these wavelengths. In order to be implemented in the delay arm, a dichroic mirror may be purchased, with HR coating on each face matched to a single wavelength as shown in figure 5.1.

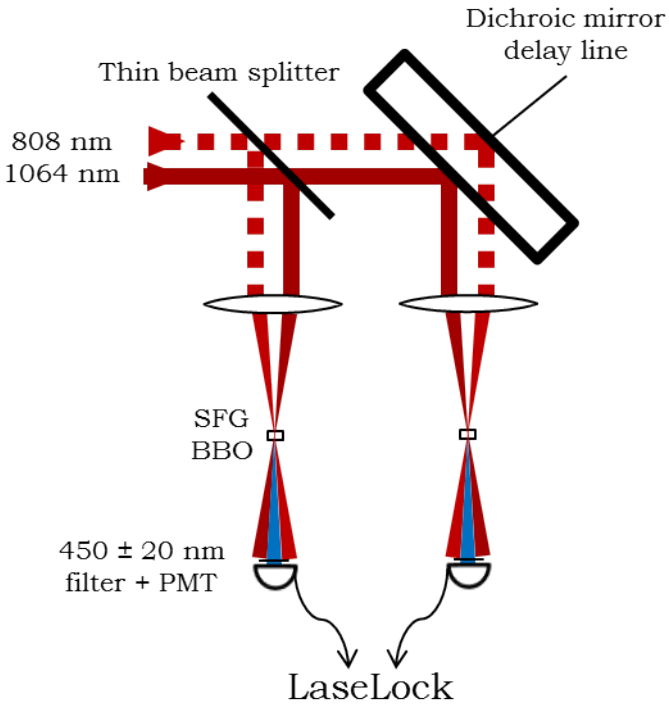

Figure 5.1: Dichroic mirror as a delay line for separating the synchronisation signals.

One aspect of the Ti:Sapphire feedback loop that may be causing issue is the mounting height; the Ti:Sapphire is mounted a few cm below the optical plane of most other optics but is gradually lifted to this plane via two turning mirrors. Additionally, the manual translation stage that supports the OC forced the beam path upward meaning that both the OC and piezo-mounted mirror have a slight vertical offset. In the context of electronic feedback provided to the mirror, a significant enough vertical or horizontal angle offset could cause walk off of the cavity mode. In turn, this may reduce the power output as a function of mirror displacement and ultimately provide negative feedback. Remounting of the Ti:Sapphire cavity and its pump to an equal height is time consuming, but may be necessary.

5.2 Future work

The compression of ultrashort pulses relies on initial characterisation and dispersion compensation for example using prisms or chirped mirrors. Prism pairs are an effective method of intra- and extra-cavity pulse compression. A proposed optical layout for the synchronous characterisation and further pulse compression of Ce:LiCAF is shown in figure 5.2. This includes a bi-directional pumping scheme that would directly pump the gain medium prior to the resonating pulse twice every round trip. The round trip of the current 3-mirror cavity involves 4 mirror reflections and 1 step in gain from the 266 nm pump. A bi-directional pumping scheme could constitute 4 mirror bounces for 2 steps in gain, or 6 mirror bounces after implementing a fourth mirror. The purpose of this bi-directional design is to increase the total 266 nm power provided to the oscillator.

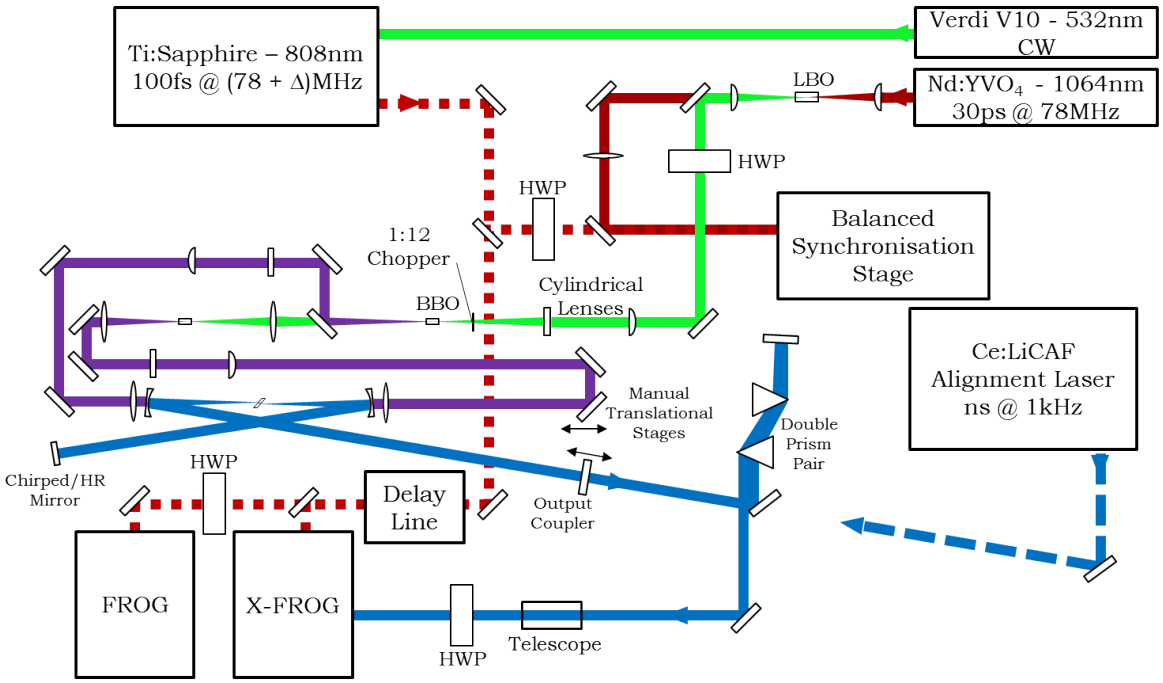

Figure 5.2: Proposed table configuration for the characterisation an construction of an efficient Ce:LiCAF KLM oscillator.

While prism pairs offer a versatile solution to pulse compression, their inherent loss in the UV increases the quality and pump requirements for lasers in this region. Chirped mirrors offer a more convenient solution over prism pairs; they exhibit less round trip loss and have the potential to compensate for higher order dispersion. The reduction in losses is simply the result of fewer optical elements, but the latter is particularly important for pulse compression

below 100 fs. Achieving this is no simple task, but is made easier via precise characterisation and design of mirror coatings. While dispersion compensating mirrors for this laser have been designed, they are yet to be fabricated and fabricating them with the required precision and low losses is a technical challenge.

References

[1] D. W. Coutts and A. J. S. McGonigle. *Cerium-doped fluoride lasers*. IEEE Journal of Quantum Electronics **40**(10), 1430 (2004).

[2] Z. L. Liu, N. Sarukura, M. A. Dubinskii, V. V. Semashko, A. K. Naumov, S. L. Korableva, and R. Y. Abdulsabirov. *Tunable ultraviolet short-pulse generation from a Ce:LiCAF laser amplifier system and its sum-frequency mixing with an Nd:YAG laser*. Japanese Journal of Applied Physics Part 2-Letters & Express Letters (1998).

[3] E. Granados, D. W. Coutts, and D. J. Spence. *Mode-locked deep ultraviolet Ce:LiCAF laser*. Optics Letters **34**(11), 1660 (2009).

[4] T. Kobayashi and Y. Kida. *Ultrafast spectroscopy with sub-10 fs deep-ultraviolet pulses*. Physical Chemistry Chemical Physics **14**(18), 6200 (2012).

[5] S. Witte, R. T. Zinkstok, W. Ubachs, W. Hogervorst, and K. S. E. Eikema. *Deep-ultraviolet quantum interference metrology with ultrashort laser pulses*. Science **307**(5708), 400 (2005).

[6] P. Baum, S. Lochbrunner, and E. Riedle. *Generation of tunable 7-fs ultraviolet pulses: achromatic phase matching and chirp management*. Applied Physics B-Lasers and Optics **79**(8), 1027 (2004).

[7] C. G. Durfee, S. Backus, H. C. Kapteyn, and M. M. Murnane. *Intense 8-fs pulse generation in the deep ultraviolet*. Optics Letters **24**(10), 697 (1999).

[8] Z. Baozhen, J. Yongliang, K. Sueda, N. Miyanaga, and T. Kobayashi. *Sub-15fs ultraviolet pulses generated by achromatic phase-matching sum-frequency mixing*. Optics Express **17**(20), 17711 (2009).

[9] S. A. Diddams. *The evolving optical frequency comb [invited]*. Journal of the Optical Society of America B: Optical Physics **27**(11), B51 (2010).

[10] S. W. D. Tsen, T. C. Wu, J. G. Kiang, and K. T. Tsen. *Prospects for a novel ultrashort pulsed laser technology for pathogen inactivation*. Journal of Biomedical Science **19**(1) (2012).

[11] P. Sowa, J. Rutkowska-Talipska, U. Sulkowska, K. Rutkowski, and R. Rutkowski. *Electromagnetic radiation in modern medicine: Physical and biophysical properties*. Polish Annals of Medicine **19**(2), 139 (2012).

[12] B. Wu and A. Kumar. *Extreme ultraviolet lithography and three dimensional integrated circuit - a review*. Applied Physics Reviews **1**(1) (2014).

[13] B. Wu and A. Kumar. *Extreme ultraviolet lithography: A review*. Journal of Vacuum Science and Technology B: Microelectronics and Nanometer Structures **25**(6), 1743 (2007).

[14] A. Fernandez, T. Fuji, A. Poppe, A. FÃijrbach, F. Krausz, and A. Apolonski. *Chirped-pulse oscillators: A route to high-power femtosecond pulses without external amplification*. Optics Letters **29**(12), 1366 (2004).

[15] A. J. De Maria, D. A. Stetser, and H. Heynau. *Self mode-locking of lasers with saturable absorbers*. Applied Physics Letters **8**(7), 174 (1966).

[16] A. K. Alhowaish, N. Dietrich, M. Onder, and K. Fritz. *Effectiveness of a 308-nm excimer laser in treatment of vitiligo: A review*. Lasers in Medical Science **28**(3), 1035 (2013).

[17] H. M. Pask, P. Dekker, R. P. Mildren, D. J. Spence, and J. A. Piper. *Wavelength-versatile visible and UV sources based on crystalline Raman lasers*. Progress in Quantum Electronics **32**(3-4), 121 (2008).

[18] E. Granados, D. J. Spence, and R. P. Mildren. *Deep ultraviolet diamond Raman laser*. Optics Express **19**(11), 10857 (2011).

[19] O. Kitzler, A. McKay, and R. P. Mildren. *Continuous-wave wavelength conversion for high-power applications using an external cavity diamond raman laser*. Optics Letters **37**(14), 2790 (2012).

[20] L. R. Elias, W. S. Heaps, and W. M. Yen. *Excitation of UV fluorescence in LaF_3 doped with trivalent cerium and praseodymium*. Physical Review B (Solid State) **8**(11), 4989 (1973).

[21] N. Sarukura, M. A. Dubinskii, Z. L. Liu, V. V. Semashko, A. K. Naumov, S. L. Korableva, R. Y. Abdulsabirov, K. Edamatsu, Y. Suzuki, T. Itoh, and Y. Segawa. *Ce^{3+}-activated fluoride-crystals as prospective active media for widely tunable ultraviolet ultrafast lasers with direct 10-ns pumping*. IEEE Journal of Selected Topics in Quantum Electronics **1**(3), 792 (1995).

[22] L. Hua, D. J. Spence, and D. W. Coutts. *Highly efficient ultra-low threshold miniature cerium fluoride lasers generating sub-nanosecond pulses at 287 nm and 311 nm*. Proceedings of the SPIE - The International Society for Optical Engineering **6100**, 610007 (2006).

[23] H. Liu, D. J. Spence, K. Johnson, D. W. Coutts, H. Sato, and T. Fukuda. *UV picosecond microchip cerium lasers*. In *Advanced Solid-State Photonics, ASSP 2007* (Optical Society of America).

[24] D. J. Spence, H. Liu, and D. W. Coutts. *Low-threshold miniature Ce:LiCAF lasers*. Optics Communications **262**(2), 238 (2006).

[25] D. J. Spence, H. Liu, D. W. Coutts, and IEEE. *Miniature Ce:LiLuF/Ce:LiCAF dual-crystal single-cavity laser pumped at 266 nm*, pp. 193–194. IEEE Lasers and Electro-Optics Society (LEOS) Annual Meeting (Ieee, New York, 2005).

[26] A. J. S. McGonigle, D. W. Coutts, and C. E. Webb. *530-mw 7-khz cerium LiCAF laser pumped by the sum-frequency-mixed output of a copper-vapor laser*. Optics Letters **24**(4), 232 (1999).

[27] A. J. S. McGonigle, D. W. Coutts, and C. E. Webb. *A 380-mw 7-khz cerium LiLuF laser pumped by the frequency doubled yellow output of a copper-vapor-laser*. IEEE Journal of Selected Topics in Quantum Electronics **5**(6), 1526 (1999).

[28] B. Wellmann, D. J. Spence, and D. W. Coutts. *Tunable continuous-wave deep-ultraviolet laser based on Ce:LiCAF*. Optics Letters **39**(5), 1306 (2014).

[29] B. Wellmann, D. J. Spence, and D. W. Coutts. *Dynamics of solid-state lasers pumped by mode-locked lasers*. Optics Express (2015).

[30] C. Bourassin-Bouchet, S. De Rossi, J. Wang, E. Meltchakov, A. Giglia, N. Mahne, S. Nannarone, and F. Delmotte. *Shaping of single-cycle sub-50-attosecond pulses with multilayer mirrors*. New Journal of Physics **14** (2004).

[31] J. D. Kafka and T. Baer. *Prism-pair dispersive delay-lines in optical pulse-compression*. Optics Letters **12**(6), 401 (1987).

[32] P. C. Wagenblast, U. Morgner, F. Grawert, T. R. Schibli, F. X. KÃďrtner, V. Scheuer, G. Angelow, and M. J. Lederer. *Generation of sub-10-fs pulses from a Kerr-lens mode-locked Cr^{3+}:LiCAF laser oscillator by use of third-order dispersion-compensating double-chirped mirrors*. Optics Letters **27**(19), 1726 (2002).

[33] M. Valadan, D. D'Ambrosio, F. Gesuele, R. Velotta, and C. Altucci. *Temporal and spectral characterization of femtosecond deep-UV chirped pulses*. Laser Physics Letters **12**(2), 025302 (7 pp.) (2015).

[34] T. R. Schibli, J. Kim, O. Kuzucu, J. T. Gopinath, S. N. Tandon, G. S. Petrich, L. A. Kolodziejski, J. G. Fujimoto, E. P. Ippen, and F. X. Kaertner. *Attosecond active synchronization of passively mode-locked lasers by balanced cross correlation*. Optics Letters **28**(11), 947 (2003).

[35] *Femtosecond Laser Spectroscopy* (Springer US: Boston, MA, Boston, MA, 2005).

[36] E. Granados, A. Fuerbach, D. W. Coutts, and D. J. Spence. *Asynchronous cross-correlation for weak ultrafast deep ultraviolet laser pulses*. Applied Physics B-Lasers and Optics **97**(4), 759 (2009).